Precambrian Research 409 (2024) 107433

Contents lists available at ScienceDirect

Precambrian Research

journal homepage: www.elsevier.com/locate/precamres

An earliest Ediacaran oxygenation episode in the Wilpena Group, Adelaide Superbasin, South Australia

Kelsey G. Lamothe [a,*], Malcolm W. Wallace [a], Ashleigh V.S. Hood [a], Catherine V. Rose [b]

[a] School of Earth Sciences, University of Melbourne, Parkville, Victoria 3010, Australia
[b] School of Earth and Environmental Sciences, University of St Andrews, Scotland KY16 9TS, United Kingdom

ARTICLE INFO

Keywords:
Neoproterozoic oxygenation
Carbonate geochemistry
Marine cements
REE + Y

ABSTRACT

The first appearance of animals during the Ediacaran is arguably related to an increase in oceanic oxygenation during this time. However, there is considerable ambiguity in the global record of Ediacaran oxygenation, making it difficult to assess the potential links between oxygen and metazoan evolution. Here, we examine the earliest Ediacaran Nuccaleena Formation cap dolomite and basal Brachina Formation of the Adelaide Superbasin, South Australia, to determine the redox landscape in which these units were deposited. Red shales are present at the base of the Brachina Formation (lower Mooloolloo Siltstone Member) over much of the Adelaide Superbasin but these transition laterally into green shales in the north, correlating with a facies transition into a deeper water setting.

Fibrous dolomite cements within sheet cavities of the Nuccaleena Formation cap dolomite display evidence of a primary marine origin. Cathodoluminescence microscopy and laser ablation ICP-MS trace element analysis of these marine dolomite cements indicates a transition from an oxic environment in the south (with low Fe, Mn, and a Ce anomaly) to an anoxic (ferruginous) setting in the north (with high Fe, Mn and no Ce anomaly). This cap carbonate trace element geochemistry is spatially consistent with the overlying red to green shale transition in the basal Brachina Formation. Together, these data suggest the existence of a deep-water chemocline in this basin, separating an oxic upper water column from a ferruginous deeper water mass. This oxic interval directly post-dates the end-Cryogenian Marinoan Glaciation and is synchronous with an earliest Ediacaran oxygenation event previously described from South China.

This evidence from the Adelaide Superbasin provides direct evidence for an earliest Ediacaran oxic water mass penetrating to a substantial paleodepth. The synchronous development of oxic intervals in both Australia and South China supports the notion of a globally developed oceanic oxygenation event and is consistent with the hypothesis that Ediacaran continental margin settings were periodically bathed in oxic water, conducive to the evolution of metazoans.

1. Introduction

The oxygenation history of Earth's atmosphere–ocean system is dominated by three major episodes; the Great Oxidation Event (2.4–2.2 Ga), the Neoproterozoic Oxygenation Event (~800–540 Ma) and a mid-Paleozoic oxygenation event (450–350 Ma) (Canfield and Teske, 1996; Holland, 2002; Dahl et al., 2010; Wallace et al., 2017). The Neoproterozoic Oxygenation Event is particularly interesting because it is associated with the appearance of the first metazoans during the Ediacaran Period (635 to ~ 541 Ma) (e.g., Narbonne and Gehling, 2003). However, the timing, nature and even existence of this Neoproterozoic rise in oxygen is often debated. Traditional models suggest a monotonic, stepped rise in atmospheric oxygen (e.g., Holland, 2006; Shi et al., 2022). A less linear rise, punctuated by multiple short-lived oxygenation events has also been proposed (e.g., Lyons et al., 2014; Sahoo et al., 2016; Tostevin and Mills, 2020). The timing of the initiation of Neoproterozoic oxygenation is also poorly constrained, with some evidence suggesting a Tonian atmospheric oxygenation event (Cole et al., 2016). However, it is likely that Neoproterozoic marine oxygenation was highly temporally and spatially heterogeneous (Reinhard et al., 2016). It appears that dominantly anoxic shallow marine conditions persisted into at least the Late Cryogenian (e.g. Hood and Wallace, 2015; O'Connell

* Corresponding author.
E-mail address: kel.lamothe@gmail.com (K.G. Lamothe).

https://doi.org/10.1016/j.precamres.2024.107433
Received 11 March 2024; Received in revised form 13 May 2024; Accepted 16 May 2024
Available online 28 May 2024

et al., 2020), and much of the deep oceans may have remained largely anoxic well into the Phanerozoic (Sperling et al., 2015, Wallace et al., 2017).

The evolutionary appearance of the Ediacaran biota has focussed much attention on the Ediacaran record of oxygenation. Enrichment of redox-sensitive metals in black shales in South China has provided evidence for an earliest Ediacaran (post-Marinoan) oxygenation event (Sahoo et al., 2012, 2016) and lends credence to the suggestion that post-glacial weathering (with consequent marine phosphorus influx) may have kick-started Ediacaran oxygenation and metazoan evolution (Hoffman and Schrag, 2002; Planavsky et al., 2010; Sahoo et al., 2012). In addition, widespread redbeds and various geochemical evidence is suggestive of oxygenation in the mid-Ediacaran, just prior to the appearance of the Ediacaran biota (e.g. Fike et al., 2006; Hardisty et al., 2017; Song et al., 2017; Zhang et al., 2019). However, on some continents, there is a distinct lack of evidence for Ediacaran oxygenation (Johnston et al., 2013; Kunzmann et al., 2015) and it has been suggested that the South China data might be anomalous and not supportive of a global, early Ediacaran oxygenation event (Johnston et al., 2013; Miller et al., 2017). Therefore, there is significant ambiguity regarding Ediacaran oxygenation and its effect on the evolution of multicellular metazoans (Ostrander, 2023).

Objections to an earliest Ediacaran oxygenation event have been largely based on the absence of evidence for this oxic episode globally (Johnston et al., 2013; Kunzmann et al., 2015; Miller et al., 2017). More generally, there is evidence from a variety of paleoredox proxies that points to the Ediacaran deep oceans not being well oxygenated (Dahl et al., 2010; Sperling et al., 2015; Wallace et al., 2017). Here, we analyse the sedimentology, stratigraphy and geochemical composition of cap carbonates and shale from the early Ediacaran Nuccaleena and Brachina formations across the Adelaide Superbasin to constrain marine redox conditions immediately following the Marinoan glaciation. This stratigraphic interval was deposited in deep subtidal (but not abyssal) conditions characterised by turbiditic and hemipelagic sedimentation. The evidence presented here indicates a period of oxic continental margin marine conditions following the end of the Marinoan glaciation.

2. Geological context

The Flinders Ranges of South Australia comprise the uplifted northern part of the Adelaide Superbasin, historically known as the Adelaide Geosyncline (Preiss, 1987; Fig. 1). This sedimentary succession of Neoproterozoic to early Paleozoic mixed carbonates and siliciclastics unconformably overlies the mid-Proterozoic crystalline basement. Deposition began ca. 830 Ma, during the rifting that preceded the breakup of Rodinia, and a nearly complete archive of Neoproterozoic sedimentation is preserved (Coats and Blissett, 1971; Preiss, 1987). The succession is exposed in a fold belt orientated north–south and the basin is thought to have deepened both to the north and also to the southeast (e.g., Preiss, 1987; McKirdy et al., 2001). The Adelaide Superbasin is divided into several structural domains, with the North Flinders Zone, Central Flinders Zone, and northern part of the Nackara Arc making up the Flinders Ranges (Preiss, 1987). Neoproterozoic strata are divided into four units: the Callanna Group and Burra Group, encompassing the Tonian strata, the Umberatana Group, consisting of the Cryogenian strata including deposits from both Neoproterozoic glaciations, and the Wilpena Group, made up of the Ediacaran strata (Preiss et al., 1998).

The Nuccaleena and Brachina formations make up the lower part of the Ediacaran Wilpena Group (Fig. 2) (Dalgarno and Johnson, 1964). These units overlie the Elatina Formation of the Yerelina Subgroup, which is the uppermost unit of the Umberatana Group, and represents the Marinoan glaciation in the Central and Northern Flinders Ranges. The age of the Marinoan glaciation and onset of cap deposition is poorly constrained in the Adelaide Superbasin but estimated to be approximately 636 Ma from correlation to the Marinoan glacial deposits in Tasmania, Australia (Calver et al., 2013). This estimate is derived from

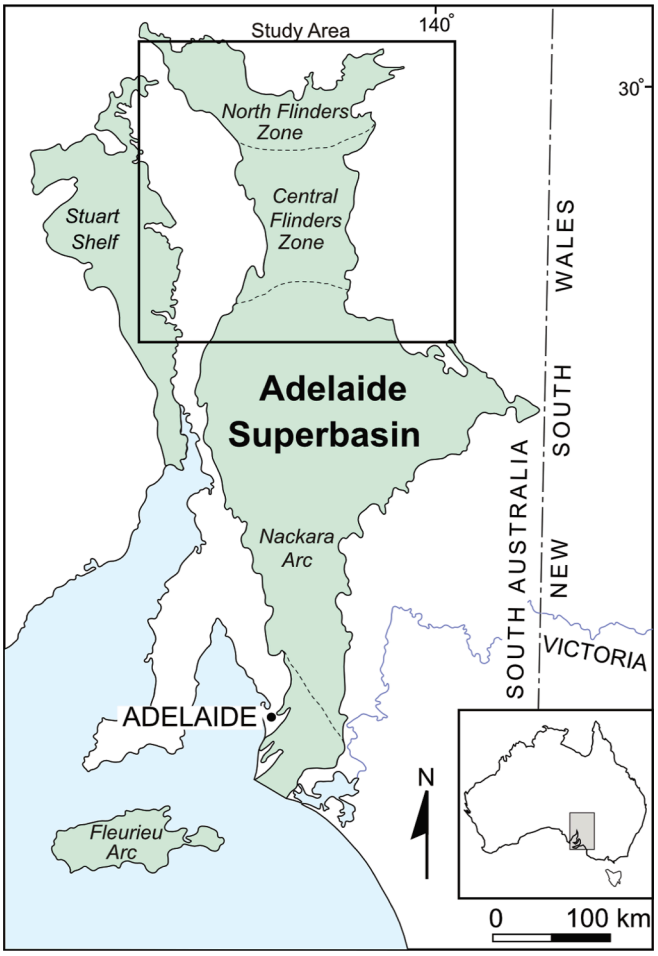

Fig. 1. General map of the Adelaide Superbasin region. Green area represents distribution of Neoproterozoic strata. (For interpretation of the references to colour in this figure legend, the reader is referred to the web version of this article.)

an age of 636.41 ± 0.45 Ma that was obtained from U-Pb dating of zircons within in the uppermost Marinoan Cottons Breccia in King Island (Calver et al., 2013). The duration of cap carbonate deposition is contentious, with estimates ranging from thousands to millions of years. Shorter estimates are made based on the high sedimentation rates assumed for the original Snowball deglaciation model, whereas longer estimates are from paleomagnetic data recording magnetic reversals in the Marinoan cap carbonates in Brazil, Oman and Australia (e.g., Hoffman and Schrag, 2002; Trindade et al., 2003; Kilner et al., 2005; Raub et al., 2007; Hoffman and Li, 2009; Font et al., 2010; Fairchild et al., 2023). Very few age constraints exist for the overlying Ediacaran strata in the Flinders Ranges. Samples from the Brachina Formation have been dated as 601 ± 68 Ma using the Rb-Sr system, though it has been determined that this date has been partially reset (Webb, 1981). The mid-Ediacaran Bunyeroo Formation hosts a horizon of ejecta from the Acraman Impact, the age of which is loosely estimated as ca. 593 ± 32 Ma by Rb-Sr shale dating (Compston et al., 1987).

The Nuccaleena Formation marks the base of the Ediacaran Period and beginning of post-glacial transgression, overlying the Marinoan glacial deposits of the Elatina Formation (Knoll et al., 2006). The Elatina Formation typically appears as a pink-red pebbly sandstone, and usually has a relatively sharp contact with the overlying cap carbonate (Preiss, 1987). The Nuccaleena Formation is described as a thin, pink-yellow laminated dolomite, ranging in stratigraphic thickness from less than a metre to 33 m (Preiss, 1987). It is laterally continuous throughout nearly the entire Flinders Ranges. The Nuccaleena Formation contains features

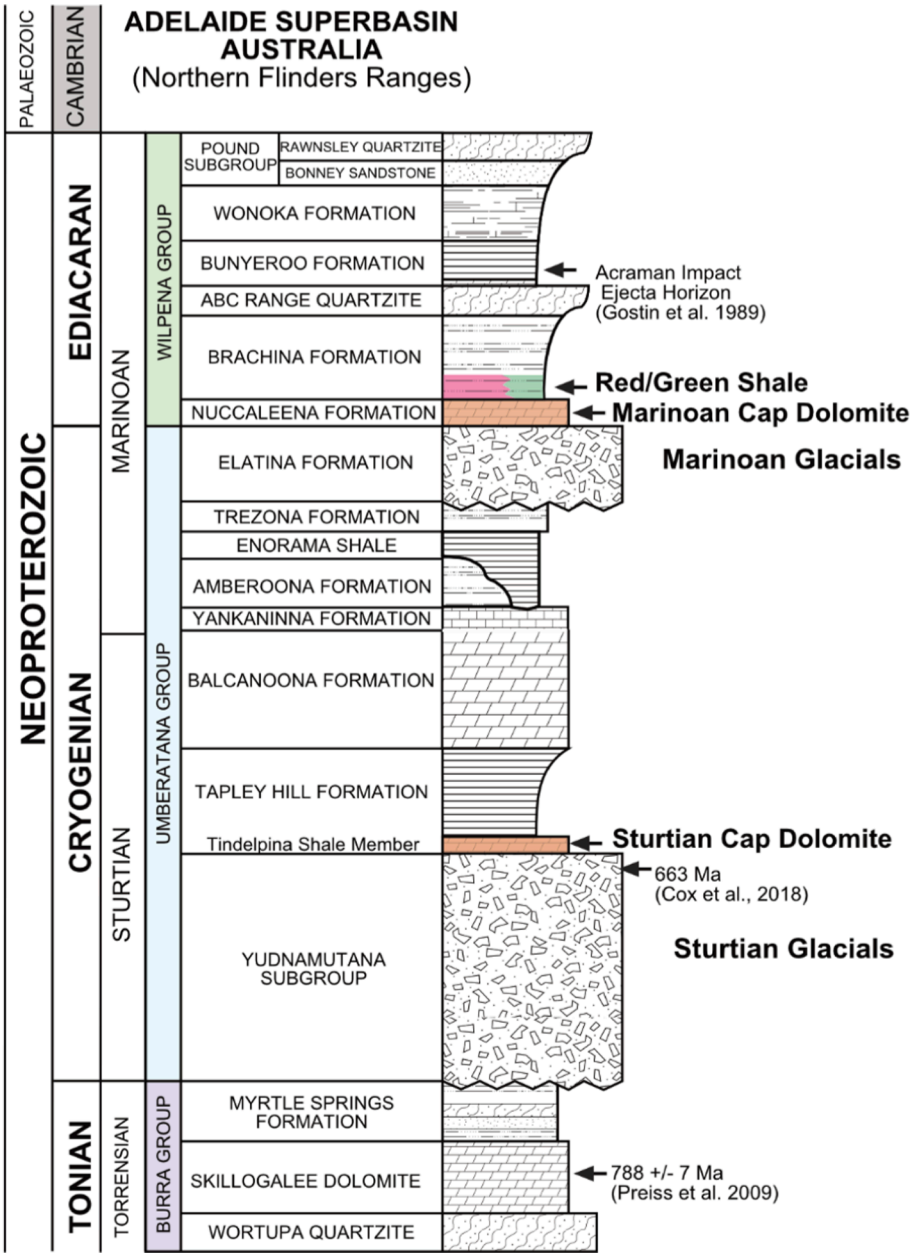

Fig. 2. Generalized stratigraphy of the Neoproterozoic succession in the Flinders Ranges.

typical of Marinoan cap carbonates globally including graded beds, sheet cavities with fibrous cements, antiformal structures–which are referred to as teepees or giant wave ripples–and flute marks (Kennedy, 1996; Rose and Maloof, 2010; Wallace et al., 2019). This formation also preserves a negative carbon isotope excursion at its base, which is variably expressed across the Adelaide Superbasin (Rose and Maloof, 2010).

The Brachina Formation conformably overlies the Nuccaleena Formation cap carbonate in the southwestern and central Flinders Ranges (Preiss, 1987). The transition between these units is characterized by an interval of interbedded nodular dolomites and shales, where carbonate content gradually decreases upwards. The Brachina Formation is composed mostly of thinly bedded siltstones with minor shale and fine-grained sandstone and is typically over a kilometre in stratigraphic thickness. The unit gradually coarsens upwards and is overlain by the ABC Range Quartzite in the central Flinders Ranges. The Mooloolo Siltstone Member at the base of the Brachina Formation is described in its type section in the Central Flinders Ranges at Mooloolo Station as approximately 500 m of olive-green siltstone overlying 100 m of red siltstone (Dalgarno and Johnson, 1964; Leeson, 1970; Plummer, 1978a; Preiss, 1987). The equivalent of the Brachina Formation in the northern Flinders Ranges is named the Ulupa Siltstone and is described as green, grey, and locally purple shales (Mirams, 1964). The Ulupa Siltstone also occurs in the eastern and southeastern parts of the Nackara Arc.

3. Methods

Stratigraphic sections of the Nuccaleena and Brachina formations were measured from twelve localities across the Central and Northern Flinders Ranges, South Australia (Fig. 3). Sheet cavities with fibrous dolomite cements were collected from seven localities of the Nuccaleena Formation, with attempts to target the thickest cement crusts. Brachina Formation shale and siltstone samples were collected from twelve localities throughout the Central and Northeastern Flinders Ranges, with sampling intervals of 1.5 to 3.0 m. Shales were collected only from areas with consistent lateral coloration and minimal indications of post-

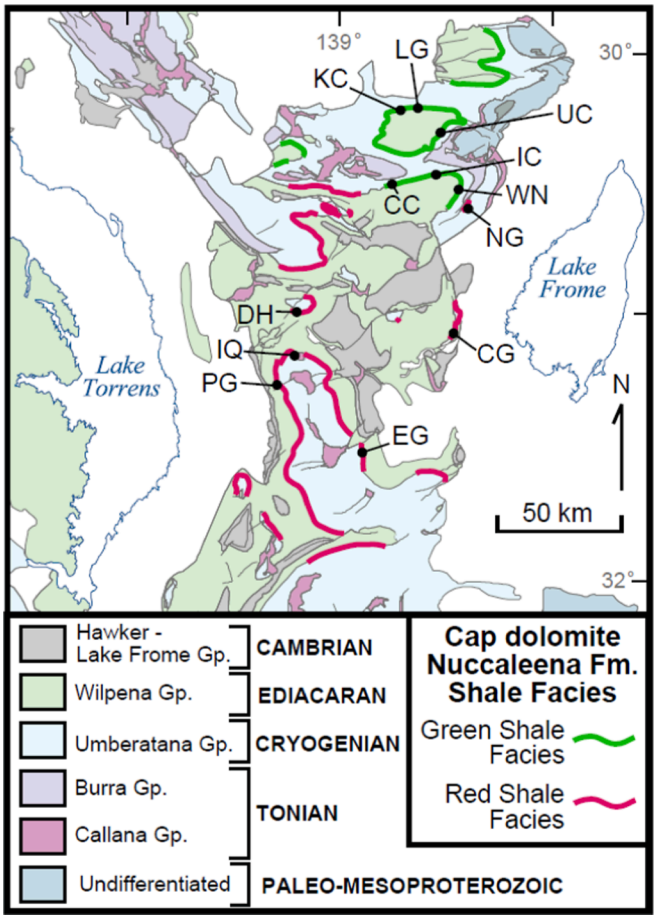

Fig. 3. Map of shale colour at contact between Nuccaleena Formation and Brachina Formation. Map modified from Rose and Maloof (2010) and Preiss (2000). Sampled localities are marked: EG = Emu Gap; PG = Parachilna Gorge; IQ = Ivy Queen Mine; CG = Mount Chambers Gorge; DH = Dunbar Hut; NG = National Park Gate; WN = Wortupa Well North; CC = Crowbar Spring Creek; IC = Idninha Creek; KC = Korrowilya Creek; LG = Lame Horse Gully.

depositional alteration (e.g., non-stratigraphic colour changes, recent weathering, veining, faulting). Stratigraphic sections were measured using a Jacob's staff through the basal red unit–where present–and several tens of metres into the overlying olive-green unit. Four sheet cavity cement localities were chosen for high-resolution geochemical analysis, with two locations from the central Flinders Ranges (Mount Chambers Gorge: CG and Ivy Queen Mine: IQ), where the Nuccaleena Formation is overlain by red shales, and two from the northern Flinders Ranges (Korrowilya Creek: KC and Lame Horse Gully: LG), where it is overlain by green shales (Fig. 3).

Cathodoluminescence microscopy was undertaken at the University of Melbourne using a Nuclide ELM2B Cathodoluminoscope attached to a Wild M400 Photomacroscope operating at 8–10 kV with a ~ 0.6 mA beam current. Laser ablation analyses were carried out on 100–200 μm thick sections that were cut from the same blocks that thin sections were made. Trace element concentration measurements were done by laser ablation-inductively coupled plasma-mass spectrometry (LA-ICP-MS) at the University of Melbourne, using a Helex 193 mn ArF excimer laser ablation system is connected to Agilent 7700x quadrupole ICP-MS. Prior to analysis, all samples were observed under cathodoluminescence to avoid diagenetic alteration, microfractures, etc. Following laser ablation, the samples were examined to determine if the ablation spot was correctly located.

Operating conditions for laser ablation analysis included a laser repetition rate of 10 Hz and an ablation time of 60 s with spot size of 100 μm. Data were reduced by Iolite Software (Paton et al., 2011) using the Trace Elements Data Reduction Scheme (Woodhead et al., 2007). Calcium was used as an internal standard element, using the calculated stoichiometric concentration for dolomite. Outliers were rejected at the ± 2 SD level. Limits of detection for the rare earth elements and yttrium (REEYs) were typically in the sub-ppb range. Internal precision (2-sigma error) for samples was generally less than ± 10 %. External reproducibility is reported as less than ± 1.6 % (2SD, n = 44) based on repeated NIST SRM612 standard measurements.

REE data are normalized to Post-Archean Australian Shale (PAAS; McLennan, 1989). The Eu anomaly was calculated as $Eu_{SN}/Eu^*_{SN} = (2*[Eu]_{SN}) / ([Sm]_{SN} + [Gd]_{SN})$ (McLennan, 1989). The Ce anomaly is quantified as $Ce_{SN}/Ce^*_{SN} = [Ce]_{SN} / (([Pr]_{SN})^2/[Nd]_{SN})$ (Lawrence et al., 2006). Middle rare earth element (MREE) enrichment is expressed as the ratio Sm_n/Yb_n, and light rare earth element (LREE) enrichment is expressed the ratio of Nd_n/Yb_n.

For colorimetry analysis, shale samples of the Brachina Formation were drilled on a fresh surface to acquire enough powder to evenly coat a 6.25 cm diameter tray. Colour measurements were performed on the powdered sample using a Konica-Minolta Chroma-Meter CR-410 colorimeter, which provides measurements of the absorbance of light (L*), the absorbance of red (a*) and the absorbance of yellow (b*). Positive values of a* represent red colours and negative values represent green colours. The absorbance of red (a*) can be used as a qualitative estimate of the hematite content of the sample.

4. Results

4.1. Distribution of sheet cavities

Sheet cavities are not always present within the Nuccaleena Formation but were observed at several localities across the Flinders Ranges (Ivy Queen Mine, Dunbar Hut, Mount Chambers Gorge, Crowbar Spring Creek, Idninha Creek, Korrowilya Creek, and Lame Horse Gully) (Fig. 3). Rose and Maloof (2010) also recorded sheet cavities at their Billy Springs locality in the Mt. Fitton region of the northern Flinders Ranges. Only four localities from this study had fibrous cements that were well preserved and thick enough for laser ablation analysis. From south to north, these four localities are Ivy Queen Mine (IQ), Mount Chambers Gorge (CG), Lame Horse Gully (LG) and Korrowilya Creek (KC) (Fig. 3).

Sheet cavities observed in this study are erratically distributed across the central and northern Flinders Ranges. The most laterally expansive outcropping of sheet cavities documented in this study occurs in Lame Horse Gully to Korrowilya Creek localities in the Northern Flinders, where the sheet cavities appear to be well developed over a significant lateral extent (kilometers). However, the Ivy Queen Mine locality in the Central Flinders has the most intense development of sheet cavities with the thickest fibrous cements. At this locality, sheet cavity development is restricted to the immediate vicinity (within 500 m) of the Oratunga Diapir. Away from the diapir, sheet cavities are completely absent within the Nuccaleena Formation. At Chambers Gorge, sheet cavities and fibrous cements of the Nuccaleena Formation are well-developed over a lateral distance of several kilometers, however, sheet cavity development is not uniform. At this locality, the cavity systems and fibrous cements appear to be better developed where the cap dolomite is thinner and more condensed. At Dunbar Hut, sheet cavities are similarly better developed where the Nuccaleena Formation is thinner.

4.2. Cement petrology

The sheet cavities in the Nuccaleena Formation are limited to the lower part of the unit, as is the case globally (Kennedy, 1996; Hoffman, 2011). The cavities are parallel to bedding, typically millimetres to centimetres thick, and can extend laterally for decimetres to metres. They are generally lined with isopachous crusts of fibrous dolomite cement up to a few millimetres thick. The final phase of cements consists

of either coarsely crystalline carbonate or silica, which directly overlie fibrous dolomite cements. Internal sediments of fine-grained dolomite are commonly present and such sediments may occur at the base of cavities underlying the fibrous cements or may overlie fibrous dolomite cements (e.g. Fig. 4C).

The fibrous cements that fill the cavities in the Nuccaleena Formation generally have a radial-fibrous texture with straight extinction and rhombic crystal terminations (Hood and Wallace, 2018). The IQ samples are mainly radial-fibrous but also contain some fascicular-optic cements. All of the fibrous cements are optically length-slow. Some sheet cavities, particularly at the Chambers Gorge locality (CG), have fibrous cements which are strongly zoned in plain light. The cements are typically rich in inclusions but contain some inclusion-poor bands that follow the rhombic crystal growth. Cements from the southern localities (IQ and CG) tend to be more inclusion-rich than those in the north (KC and LG).

Cathodoluminescence (CL) microscopy shows that there are significant differences in luminescence character between sheet cavity cements from the four localities. Bright luminescence is characteristically indicative of high Mn content, whereas Fe quenches luminescence and, consequently, cements with high concentrations of Fe are typically expressed as dull-luminescent (Barnaby and Rimstidt, 1989).

The IQ fibrous cements variably show a thin zone of red luminescence along the cavity margin or in the early part of the cement crust (Fig. 5D). This red luminescent cement commonly has a diffuse or mottled character, but occasionally it is characterized by several thin bright-luminescent zones. Following this, the majority of fibrous cements are uniformly non-luminescent (Fig. 5D). The latest generation of fibrous cements are brightly luminescent with a mottled appearance. Fractures in the cements also appear bright red luminescent.

The Mount Chambers Gorge (CG) sheet cavities are generally either brightly- or non-luminescent and display strong zonation (Fig. 5B). Some cements from this locality have a patchy mottled luminescence. The Lame Horse Gully (LG) and Korrowilya Creek (KC) cements have a similar character. Both sample sets can have well-developed sheet cavities lined with crusts of fibrous dolomite cement (Fig. 4B). The crusts are typically several millimetres thick. The cements show non– to bright-cathodoluminescence zoning, with KC samples often having a slightly more mottled appearance.

4.3. Contamination and alteration

Due to the low concentrations of trace elements in marine carbonates, the primary marine geochemical signature can be easily eclipsed by any silicate or oxide detrital material that may be present. By using fibrous dolomite cements of the Nuccaleena Formation, rather than detrital sediment, this detrital contamination can be largely avoided. In addition, the cements were examined under cathodoluminescence to identify the least-contaminated and least-altered areas, which were then targeted for geochemical analysis. Concentration cutoffs of Al (<100 ppm), Th (<0.5 ppm), and total rare earth element concentration: REE_{tot} (<10 ppm) were used to screen out measurements that were likely to have been contaminated with non-carbonate material (Fig. 6).

Cathodoluminescence microscopy of the fibrous cements showed that fine-scale compositional zonation has been preserved (Fig. 5B), which serves as an indication that the cements have not undergone significant alteration or recrystallisation. Furthermore, the rare earth elements are a relatively robust paleoproxy and are unlikely to be altered during diagenesis, particularly when the Fe and Mn zonation (e.g. visualised under CL) has not been affected (Banner and Hanson, 1990).

4.4. Major and trace element concentrations

The fibrous cements of the Nuccaleena Formation vary

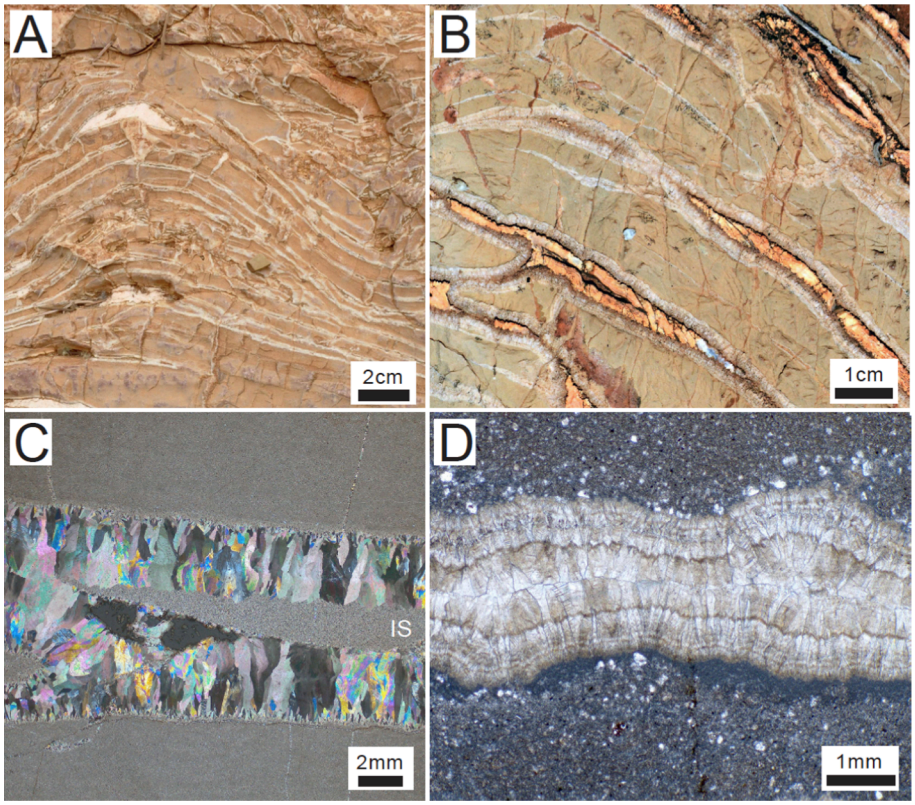

Fig. 4. Sheet cavities in the Nuccaleena Formation. A: Outcrop photograph at Mount Chambers Gorge (CG). B: Outcrop photograph at Lame Horse Gully (LG). C: Thin section photomicrograph in cross-polarized light of a sheet cavity from Ivy Queen Mine (IQ). IS = internal sediment. D: Thin section photomicrograph in plane polarized light.

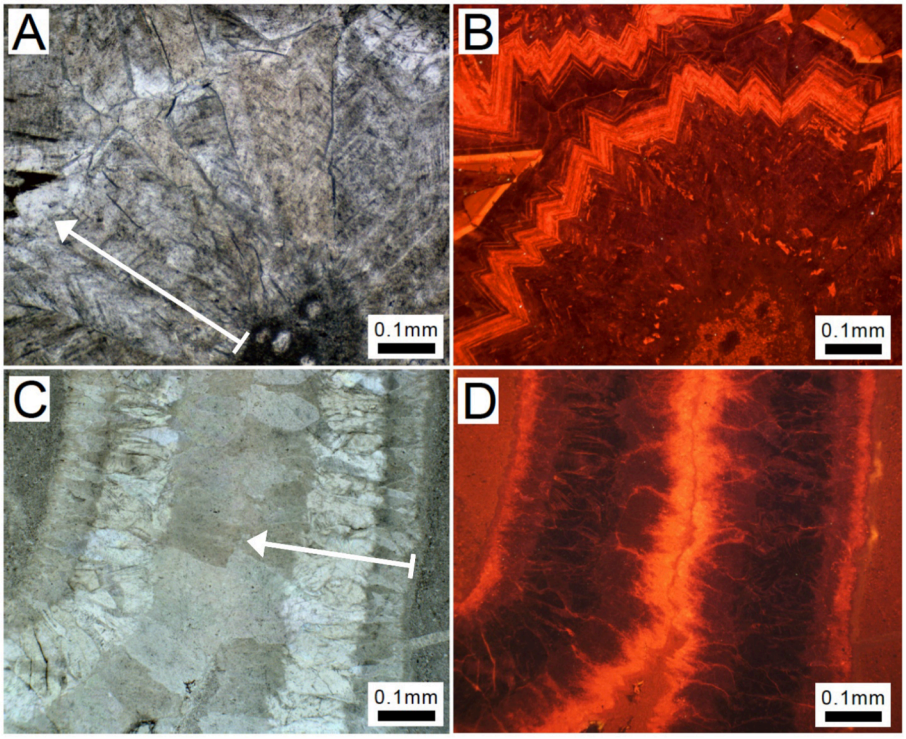

Fig. 5. Plane polarized light (PL) and cathodoluminescence (CL) photomicrographs of sheet cavity cements of the Nuccaleena Formation. White arrows in A and C indicate growth direction of the cements; perpendicular line at base of arrows marks the margin of the cavities. A: PL, Mount Chambers Gorge. B: CL, Mount Chambers Gorge, showing finely zoned cements near the centre of the sheet cavity and more mottled cements near the margin. C: PL, Ivy Queen Mine. D: CL, Ivy Queen Mine.

geochemically from south to north, across the Flinders Ranges (Fig. 7). Metal concentrations are generally lowest in the Ivy Queen (IQ) locality compared to higher values in more eastern localities (CG) and highest in northern localities (KC and LG). The lowest Fe concentrations occur in IQ samples (n = 38), with a mean value of 842 ± 688 ppm (Fig. 7). Fe increases slightly at CG (n = 28; mean 1315 ± 676 ppm), and is highest at KC (n = 7) and LG (n = 36) (means of 2400 ± 472 ppm and 2883 ± 2450 ppm, respectively).

Similarly, Mn concentrations are lowest in IQ samples, with a mean of 242 ± 228 ppm, but are notably higher in CG samples with a mean of 961 ± 702 ppm. KC and LG have Mn concentrations of 504 ± 188 ppm and 691 ± 767 ppm, respectively. Co concentrations show covariance with Mn concentrations (Fig. 8), and are highest in CG (mean of 3.9 ppm), followed by IQ (mean of 1.0 ppm), then lowest in KC and LG (means of 0.4 and 0.5 ppm, respectively).

The chalcophile elements–Zn, Pb, and Cd–are, on average, lowest in IQ samples (southernmost locality) with means of 16.8 ppm, 1.16 ppm and 0.22 ppm, respectively. Mean concentrations for these elements are variably higher in the more northern localities. Ba and Sr concentrations are both significantly lower in IQ and CG samples when compared to KC and LG, with the difference being more pronounced in Ba. The mean Ba concentrations in IQ and CG are 4.0 ± 3.6 ppm and 1.7 ± 0.4 ppm, respectively, and in KC and LG are 9.0 ± 4.9 ppm and 21.7 ± 6.8 ppm respectively.

U concentrations are highest in IQ samples (Fig. 8), with a mean concentration of 0.9 ± 0.4 ppm. CG, LG, and KC have means of 0.3 ± 0.3 ppm, 0.4 ± 0.2 ppm, and 0.5 ± 2 ppm respectively.

4.5. Rare earth element geochemistry

Shale-normalised rare earth element profiles of the Nuccaleena Formation are quite variable between localities (Fig. 9). Variability is also recorded within individual samples, with REE profiles of the fibrous cements showing gradual changes from earliest cements along the cavity margin, towards later cements in cavity centres (Fig. 10). The average Ivy Queen normalised cement profile (4 samples, 21 spots analysed) shows LREE depletion, a negative Ce anomaly (mean $Ce/Ce^* = 0.80$) and a positive Y/Ho ratio. Moving through the cement crust from the cavity margins, IQ shows a progressive depletion in REE concentration, relative enrichment in MREE (mean Sm/Yb = 2.26 ± 1.24) and gradual depletion in HREE. Strongly negative Ce anomalies are only present in the earliest cements.

The Mount Chambers Gorge average normalised profile (5 samples, 19 spots) shows enrichment in MREE (mean Sm/Yb = 2.52 ± 1.24), a slight positive Ce anomaly (mean = 1.11) and a high Y/Ho anomaly. The Y/Ho ratio is highest in the earliest cements and decreases through the cement crust. Additionally, the HREE become progressively depleted moving inward from the margins.

The shale-normalised REE profiles of Korrowilya Creek (KC) (2 samples, 8 spots analysed) and Lame Horse Gully (LG) (5 samples, 27 spots analysed) are very similar. Both average profiles appear relatively flat with only a minor MREE enrichment (mean Sm/Yb = 0.87 ± 0.62 and 1.39 ± 0.80 respectively), but with pronounced Eu (mean = 1.394 and 1.348) anomalies and strong Y/Ho ratios. The LG cements become more REE depleted and show progressive HREE depletion and a weaker Y/Ho ratio through the later parts of the cement crust.

4.6. Shale colour distribution

The transition from the Nuccaleena Formation to the Brachina Formation is characterised by gradually increasing shale content and decreasing carbonate content. This transitional shale, and the lower shale and silt of the Brachina Formation is consistently red-coloured in the Central Flinders Ranges. The stratigraphic thickness of the red shale decreases to the north and becomes grey-black or more commonly green-coloured in the Northern Flinders Ranges (Fig. 3). The lithology of

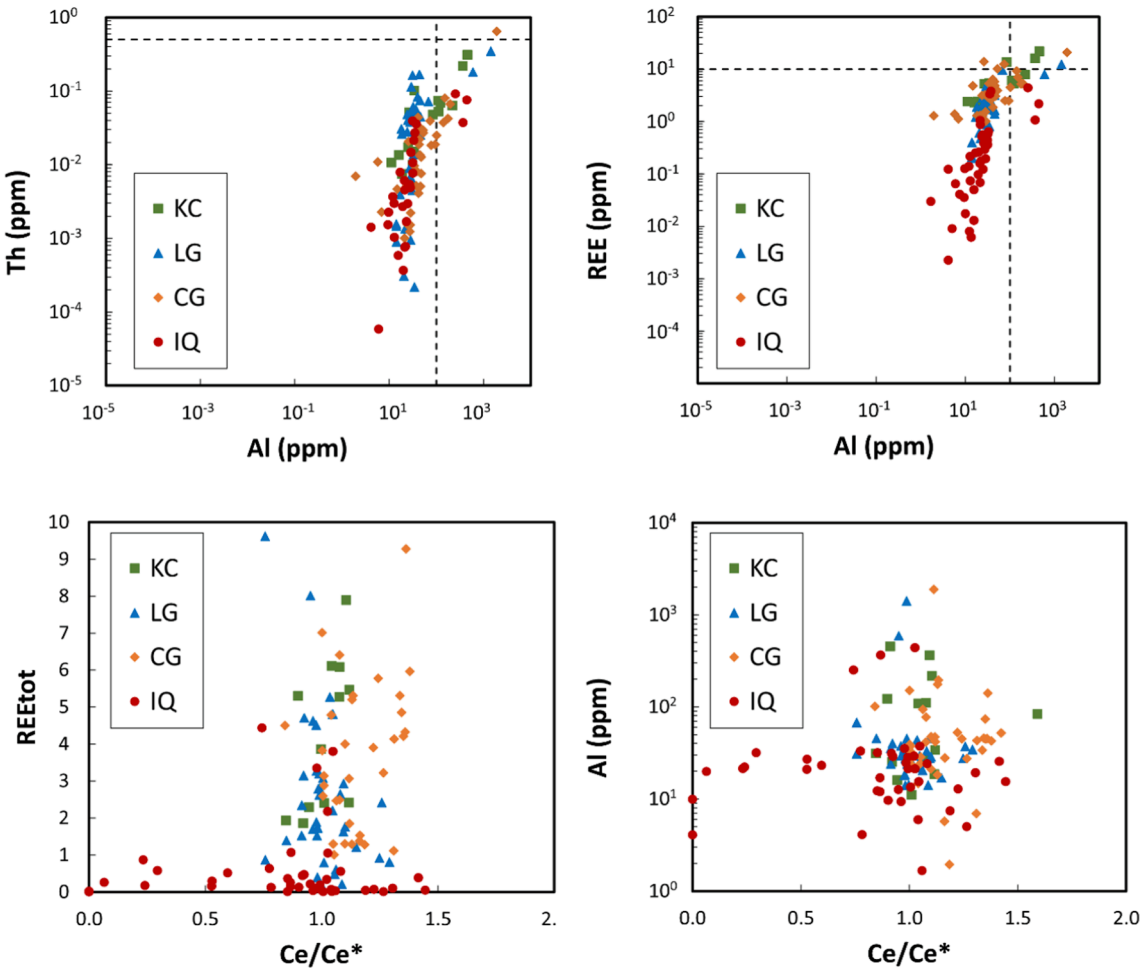

Fig. 6. Th vs. Al, REE_T vs. Al, REE_T vs. Ce anomaly, and Al vs. Ce anomaly for Nuccaleena Formation marine cement analyses. Th vs. Al and REE_T vs. Al show contamination cut-off thresholds; data points above these thresholds were not used. REE_T vs. Ce anomaly and Al vs. Ce anomaly plots show no covariance, demonstrating that Ce anomalies seen in the data set are unlikely to be related to contamination. CG = Mount Chambers Gorge; LG = Lame Horse Gully; IQ = Ivy Queen Mine; KC = Korrowilya Creek (see Fig. 3).

this interval also varies from south to north, with the southern localities having abundant thin siltstone-fine sandstone beds. These coarser beds gradually disappear northwards, with the northernmost localities being dominated by shales (also observed by Plummer, 1978a).

The red coloured shale or siltstone at the base of the Brachina Formation has been defined as the lower portion of the Mooloolo Siltstone Member (Leeson, 1970). Its thickness is variable, being documented as approximately 100 m in its type section at Bitter Springs Creek (Preiss, 1987). Sections measured in this study show the red unit to be gradually thinning to the north until it ultimately disappears (Fig. 3). In addition to the red unit thinning, the measured redness of the unit (a*) systematically decreases moving northward (Fig. 11). This red/green transition can also be observed regionally on satellite imagery (Fig. 12).

One section from the northern Flinders Ranges (NP) did not precisely follow this pattern, showing a thin red shale unit approximately 10 m thick overlying the Nuccaleena Formation (Fig. 11). However, this locality, National Park Gate (NP), is located on the eastern side of the major Paralana Fault, where it is likely that significant sinistral displacement has occurred (Preiss, 1987).

The basal-Ediacaran red beds are not the first red beds to occur in the Adelaide Superbasin. The Angepena Formation in the northern Flinders Ranges, deposited during the Cryogenian interglacial interval, is a very consistently red-coloured unit that records an oxic peritidal depositional environment influenced by flooding by ferruginous seawater (Preiss, 1987; O'Connell et al., 2020). The Amberoona Formation in the northeastern Flinders Ranges, also deposited during the Cryogenian interglacial interval in a subtidal (but still shallow) marine environment, is typically grey-green in colour but has localized red-coloured facies (Preiss, 1987). Therefore, though Cryogenian red sediments are present in the Adelaide Superbasin, they tend to be either deposited in nearshore-shallow environments or more localized. In comparison the red shales at the base of the Brachina Formation are widespread across the Central Flinders Ranges, thinning to the north (Fig. 3).

5. Discussion

5.1. Origin of sheet cavities and fibrous dolomite cements

Sheet cavities or "sheet cracks" that are partially filled by fibrous dolomite cements have been described from many Marinoan cap dolomite successions globally (e.g. Plummer, 1978b; Kennedy et al., 2001; Jiang et al., 2006; Corkeron, 2007; Hoffman and MacDonald, 2010). The fibrous dolomite cements from the Nuccaleena Formation are radial fibrous and optically length-slow, consistent with a primary dolomite mineralogy (Hood and Wallace, 2012, Hood and Wallace, 2018). Preserved primary growth zonation within the cements under cathodoluminescence (most striking at Mount Chambers Gorge locality, Fig. 5B) also suggests that the primary chemistry has been preserved. The observation of dolomite internal sediments that overlie the fibrous cements (e.g. at the Ivy Queen locality, Fig. 4C) suggests precipitation

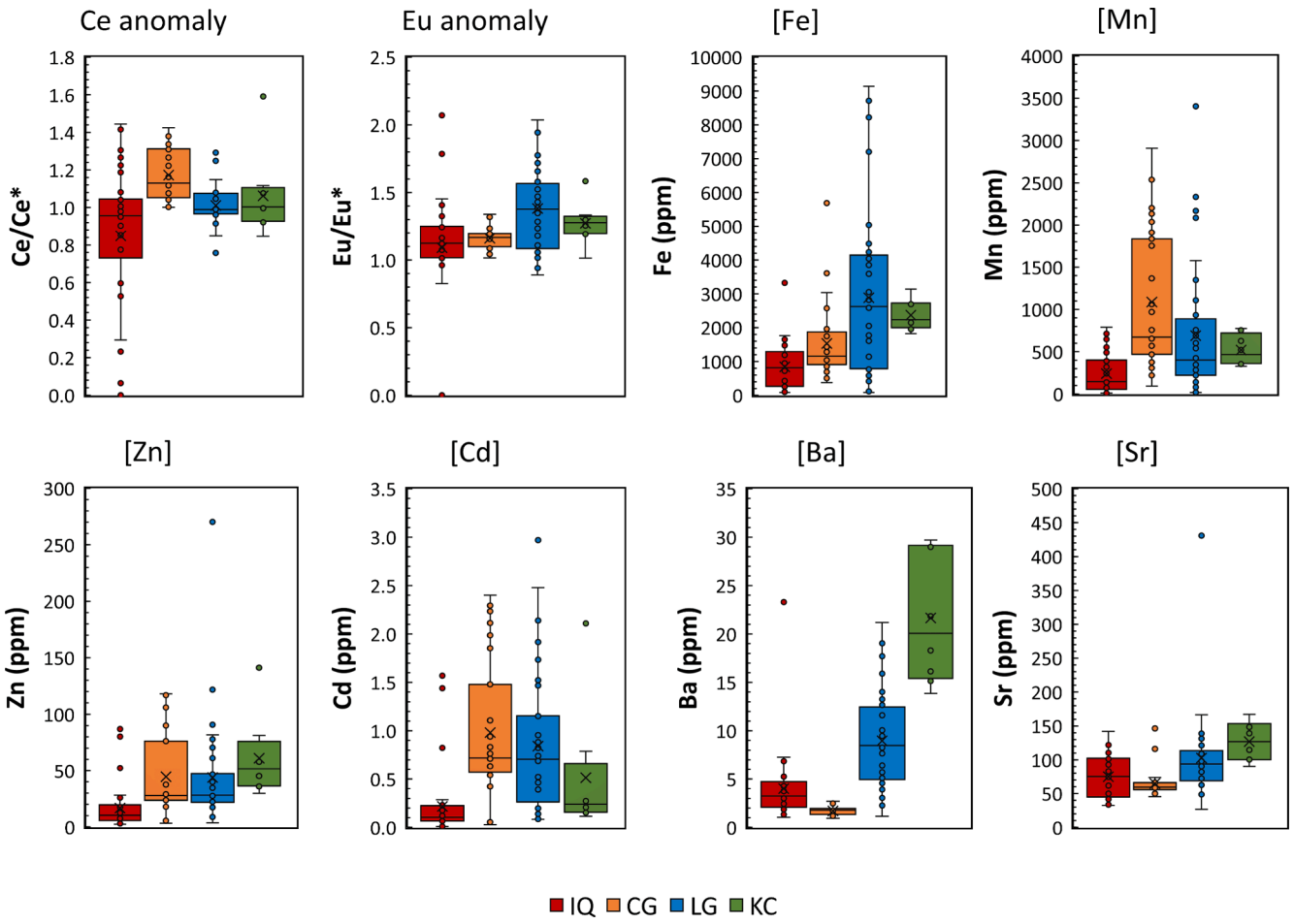

Fig. 7. Box plots showing selected trace and major element concentrations in Nuccaleena Formation marine cements at four localities. Boxes show interquartile range (with median marked by a horizontal line) and whiskers show range; data points outside of box and whiskers are outliers. CG = Mount Chambers Gorge; LG = Lame Horse Gully; IQ = Ivy Queen Mine; KC = Korrowilya Creek (see Fig. 3).

within the marine environment (Wallace et al., 2019).

Several origins have been suggested for the sheet cavities found in Marinoan cap dolomites globally. Kennedy et al. (2001) proposed that the sheet cavities, breccias, and tepees of Marinoan cap dolomites were related to methane-associated cold-seep facies (Kennedy et al., 2001; Jiang et al., 2003). Jiang et al. (2006) similarly suggested that sheet cavities from the Doushantuo Formation cap dolomite were formed by gas or fluid injection into a low permeability cohesive sediment. In contrast, Hoffman and MacDonald (2010) suggested that the sheet cavities were a result of pore fluid overpressure produced by sea level fall that was associated with ice-sheet collapse. With a similar regression-related scenario, Zhou et al. (2010) proposed that some cap dolomites had been exposed subaerially and that cavities in the cap dolomites were partially the result of karstification. Developing this hypothesis further, Gan et al. (2022) suggested that sheet cavities in the Doushantuo cap carbonate were entirely produced by karstic dissolution. Wallace et al. (2019) instead proposed that the sheet cavities may be produced by marine cementation and the force of crystallization during dolomite precipitation, causing de-lamination in partially-cemented carbonates.

In terms of the suggested origins of the fibrous dolomite cements globally, some earlier researchers suggested a cold-seep/methane related origin for the fibrous cements (Jiang et al., 2003; 2006; Wang et al., 2008). However, this was contradicted by later work indicating that the light carbon isotope signature of some cap carbonates was produced by a later hydrothermal/late diagenetic overprint (Bristow et al., 2011). Shields (2005) suggested that dolomitization and cementation of cap dolomites may have been related to a meltwater plume (plumeworld hypothesis). However, with the advent of more detailed petrological and geochemical work, there is now an emerging consensus on the synsedimentary marine origin for many Neoproterozoic fibrous dolomite cements (e.g., Hood and Wallace, 2018; Wallace et al., 2019; Hu et al., 2023). This interpretation is based on (Hood and Wallace, 2018):

1. The fibrous and inclusion-rich nature of the cements is similar to many Phanerozoic marine cements,
2. The observation of internal sediments overlying cements,
3. The length-slow optical character of the cements, which is consistent with precipitation as primary dolomite,
4. The preserved primary cathodoluminescence growth zonation within the cements.

Rose and Maloof (2010) categorized the sheet cavity-bearing dolomites of the Nuccaleena Formation as being related to a particular facies (silt ribbons and sheet crack cement facies). They suggested that the sheet cavity facies is restricted to the Northern Flinders Ranges. However, here we have documented that well-developed sheet cavities also occur within the central Flinders Ranges, as observed at the Ivy Queen mine and Mount Chambers Gorge localities. Though sheet cavities have previously been documented mainly in the north, it appears more likely that local sedimentological factors control the development of sheet cavities within the Nuccaleena Formation. From fieldwork, it appears that the presence of local paleohighs is correlated with greater

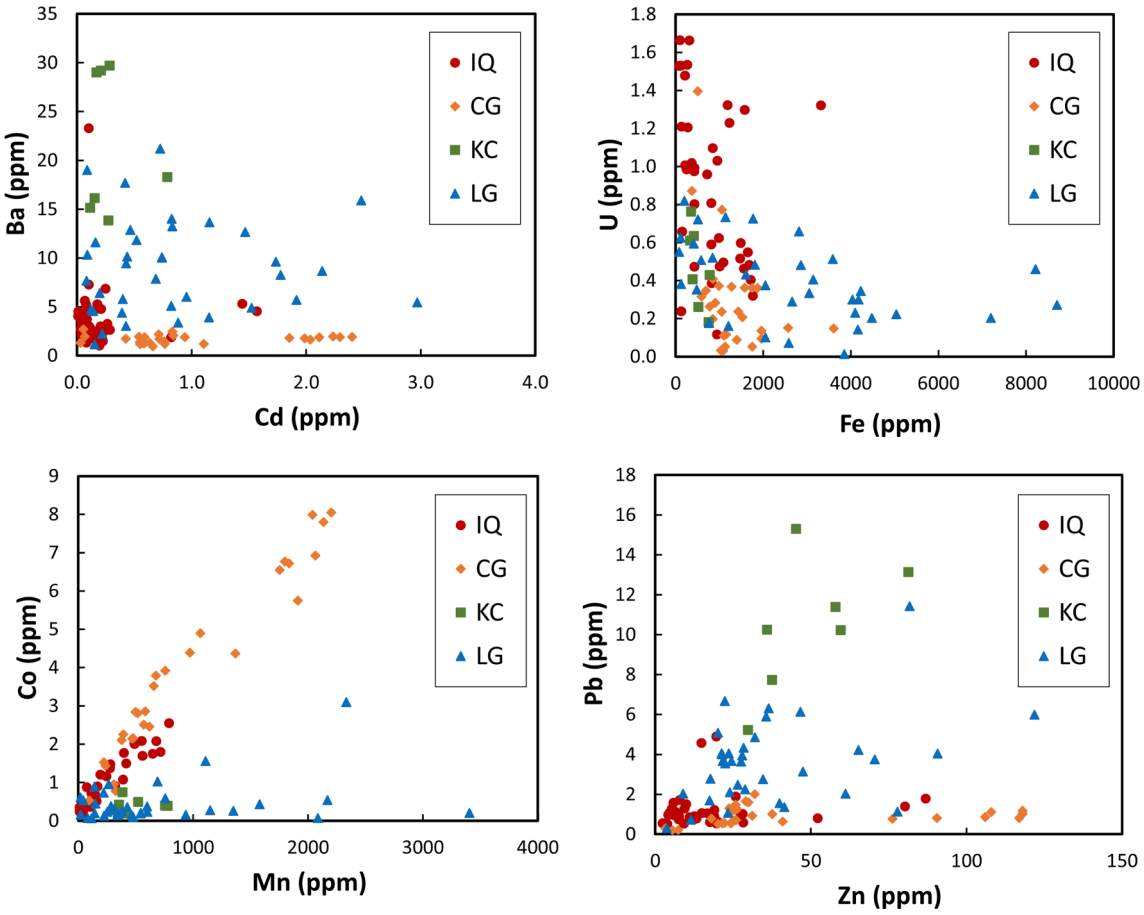

Fig. 8. Trace element crossplots from the Nuccaleena Formation marine cements. CG = Mount Chambers Gorge; LG = Lame Horse Gully; IQ = Ivy Queen Mine; KC = Korrowilya Creek (see Fig. 3).

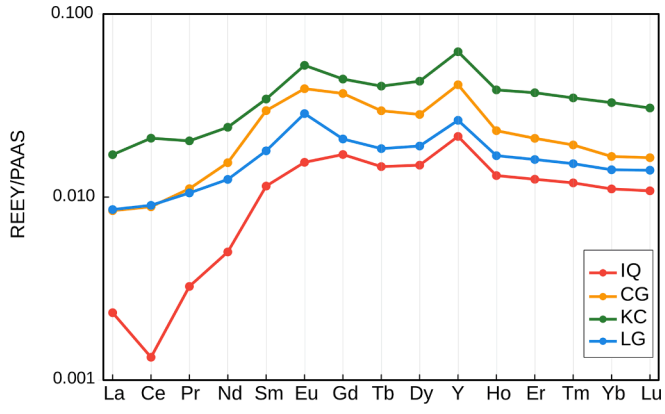

Fig. 9. Averaged PAAS-normalised REE profiles of Nuccaleena Formation fibrous dolomite cements for each of the four main localities (Fig. 3; CG = Mount Chambers Gorge; LG = Lame Horse Gully; IQ = Ivy Queen Mine; KC = Korrowilya Creek).

development of sheet cavities. This observation is particularly evident at the Ivy Queen Mine, where sheet cavities are only developed in close proximity to the Oratunga Diapir. The Oratunga Diapir has evidence of synsedimentary activity during the Cryogenian-Ediacaran (Lemon, 1988) and this may suggest that there was a local paleohigh in the vicinity of the diapir. At other localities, sheet cavities tend to be better developed where the Nuccaleena Formation is thinner (e.g. more condensed), again consistent with the presence of a local paleohigh. Hence, sheet cavities may be better developed where there is a paleohigh that leads to condensation of the cap carbonate and slower sedimentation rates. Slower sedimentation rates would be more conducive to marine cementation and displacive crystallization (Wallace et al., 2019).

5.2. South-North Paleodepth-Redox gradient

Beginning in the Late Cryogenian, there is a general paleogeographic trend of deepening to the north and to the southeast within the Adelaide Superbasin (Preiss, 1987; Fromhold and Wallace, 2012; McKirdy et al., 2001; Rose and Maloof, 2010). The south to north deepening trend is recorded in the central to northern Flinders Ranges. The late Cryogenian Etina Formation of the Central Flinders Ranges is a shallow subtidal carbonate unit (Preiss, 1973) that also displays evidence of deposition within a tidal setting (Lemon, 1988). This unit is generally agreed to be a lateral equivalent of the deeper subtidal Amberoona Formation of the Northern Flinders Ranges (Preiss, 1987; Fromhold and Wallace, 2012). Similarly, the Ediacaran ABC Range Quartzite of the Central and Southern Flinders Ranges commonly contains herringbone cross-stratification and mudcracks, indicative of shallow subtidal and intertidal conditions (Preiss, 1987). The lateral equivalent of the Brachina Formation and ABC Range Quartzite in the Northern and Eastern Flinders Ranges is the Ulupa Siltstone, which consists of olive-green siltstones and has been interpreted as being deposited in a deep subtidal setting (Preiss, 1987).

This south to north deepening trend is also consistent with the basal lithologies observed in the Mooloolo Siltstone Member. The gradual disappearance of siltstone and fine-sandstone beds in this unit northwards suggests a more basinward setting for the Northern Flinders

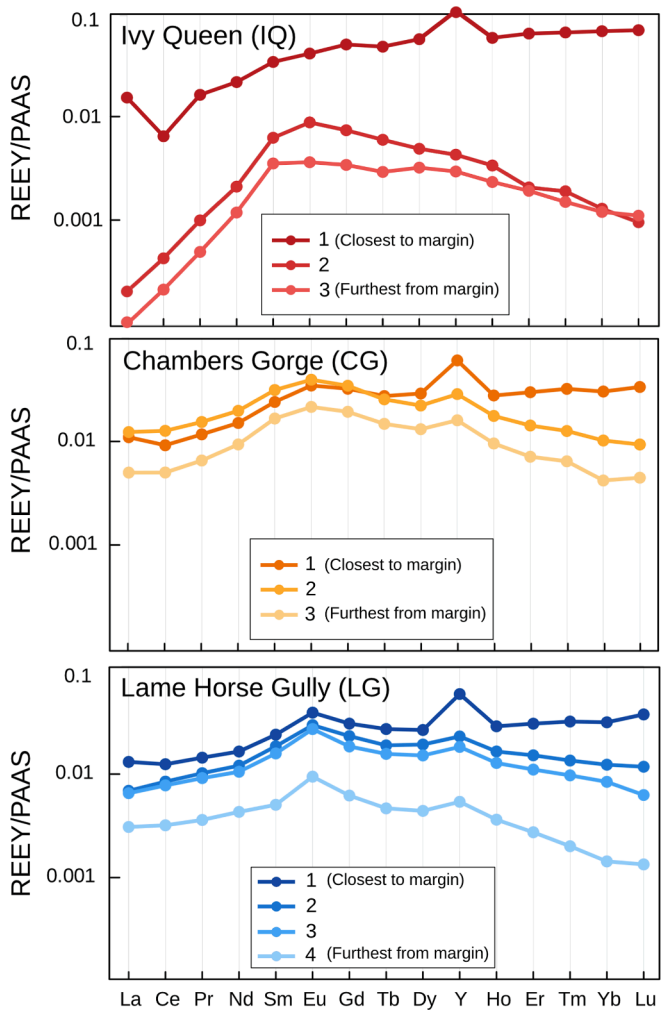

Fig. 10. PAAS-normalised REE profiles of fibrous dolomite cements of the Nuccaleena Formation at the IQ, CG and LG localities (Fig. 3).

Ranges (Plummer 1978a). The thin siltstone-fine sandstone beds of the Mooloolloo Siltstone Member, which are graded and contain flute casts, have previously been interpreted as being deposited from traction currents (Plummer, 1978a). These event beds are now more logically interpreted as thin-bedded turbidites deposited in a deep sub-wave base setting. The disappearance of these beds northwards suggests a deeper basinal setting (perhaps dominated by hemipelagic deposition) beyond the reach of most turbidity currents for the Northern Flinders Ranges. This deep water depositional setting for the Mooloolooo Siltstone Member and Ulupa Siltstone is also consistent with stratigraphic and sequence stratigraphic interpretations for the basal Wilpena Group (Preiss, 1987; 2000; Dyson, 1992; 2002).

The very consistent south to north change in the colour of shales overlying the Nuccaleena Formation directly correlates with the interpreted paleodepth gradient, with red shales being present in the southern shallower turbidite facies and green/grey/black shales present in the northern deep water facies. The colour change from red to green is caused by the disappearance of finely dispersed hematite within the shale in the northern facies. The simplest explanation for this correlation between hematite presence/absence and paleodepth is the existence of a Fe^{2+} / Fe^{3+} redox chemocline within the basin.

Below this redox chemocline, in the north, anoxic seawater conditions mean that iron will be present as Fe^{2+} and remain in solution. Above the chemocline, in the south, where more oxic conditions prevailed, ferrous iron in the water column was oxidized to ferric iron (Fe^{3+}) and precipitated as Fe oxyhydroxides, which can later convert to hematite. The absolute paleodepth of this interpreted chemocline is difficult to estimate but must be in deep subtidal conditions, significantly greater than storm wave base, as indicated by the total absence of hummocky cross-stratification or any other oscillatory-flow-produced structures (Harms et al., 1975), within the lower Mooloolloo Siltstone Member in the study area. The red/green shale transition occurs in the Mooloolloo Siltstone Member where it is dominated by shales and has no turbiditic siltstone beds, suggesting that the chemocline was located offshore from a turbidite fan and within a dominantly hemipelagic shale facies. This observation further suggests a deep subtidal environment for the Northern Flinders Ranges.

Major and trace element concentrations from the fibrous marine cements of the underlying Nuccaleena Formation are also consistent with a northward deepening trend across the basin. Iron concentrations are lowest in the southern sections, IQ and CG, and increase to the north in sections LG and KC. In shallower, more oxygenated environments above the Fe^{2+} / Fe^{3+} redox chemocline, Fe is removed from solution as Fe^{3+} and incorporated into Fe-oxyhydroxides precipitating from seawater. In lower-O_2 environments, iron remains in solution as Fe^{2+} and becomes incorporated in marine carbonate precipitates. Hence, the iron content of marine cements from the Nuccaleena Formation provides direct evidence for the existence of a deep-water ferruginous water mass overlain by a shallow oxic water mass.

The low levels of Mn and non-luminescent character of the marine cements from IQ (southernmost locality) are also consistent with formation in shallow oxic conditions where manganese is removed from solution as Mn^{4+} and precipitated as Mn oxyhydroxides.

At CG, high Mn concentrations together with strongly zoned bright and non-luminescent cements indicates slightly less oxygenated conditions around the Mn^{2+} / Mn^{4+} boundary. The northern localities (LG and KC) have moderate levels of manganese, indicating relatively reduced marine redox conditions, where Mn^{2+} is present in solution and can be incorporated into carbonates.

Barium has significantly lower concentrations in the southern localities (IQ and CG). This observation is likely related to Ba reacting with marine sulphate to form barite. Sulphate can be present under relatively oxic conditions, again consistent with the shallower, more oxic setting for the southern localities. The high Ba concentration in the northern localities indicates an absence of dissolved sulphate, consistent with a deeper water anoxic ferruginous setting. Sr concentrations behave similarly to Ba concentrations, as Sr can also be incorporated into barite.

The significantly lower total REE concentrations found in the IQ samples (southernmost locality) relative to the other three sample sets further suggest that the Ivy Queen mine locality represents an oxic environment where precipitating Mn-Fe oxyhydroxides have scavenged REE (Fig. 6) (De Baar et al., 1988). This REE depletion is not seen in CG samples, so it is likely that the Mount Chambers Gorge locality represents an environment much closer to the Mn redoxcline, where Mn-Fe oxides are cycling between precipitation and dissolution. IQ and CG (southern localities) also show an enrichment in Co that is consistent with a shallow, oxic depositional environment (Fig. 8). This enrichment is particularly strong in CG samples, which is consistent with CG being near the Mn^{2+}/Mn^{4+} chemocline, as Co has a strong affinity for Mn oxyhydroxides, seen by the covariance of these elements (Calvert and Pedersen, 1993; Hood and Wallace, 2015). Uranium concentrations are highest in IQ (southernmost locality), which is also consistent with an oxic setting, as U is soluble in its oxidised state (VI) and insoluble in its reduced state (IV) (Langmuir, 1978).

Zn, Pb and Cd have lower concentrations within cements from the southernmost (IQ) locality and are generally higher in more northward localities (being most elevated at CG). The distribution of these chalcophile elements somewhat follows Mn, and this may suggest that these elements are associated with Mn oxyhydroxides, perhaps being released to solution when Mn oxyhydroxides are dissolved below the Mn^{2+}/Mn^{4+} chemocline. The elevated values for these elements in the northern localities suggest that the seawater conditions were not euxinic, because

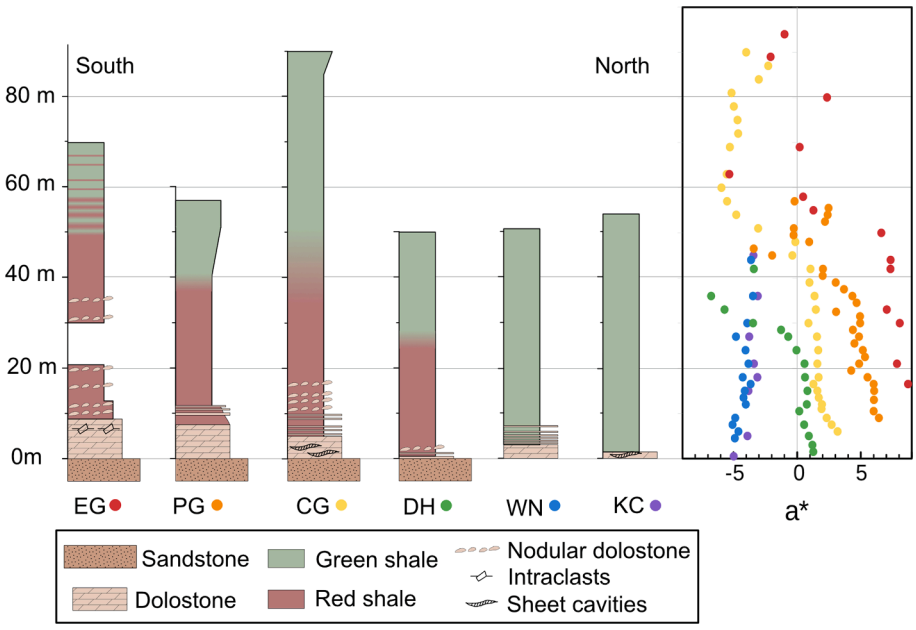

Fig. 11. Selected measured sections of the red shale/siltstone unit at the base of the Brachina Formation, and the associated a* (redness) values. EG = Emu Gap; PG = Parachilna Gorge; CG = Chambers Gorge; DH = Dunbar Hut; WN = Wortupa Well North; KC = Korrowilya Creek (see Fig. 3). (For interpretation of the references to colour in this figure legend, the reader is referred to the web version of this article.)

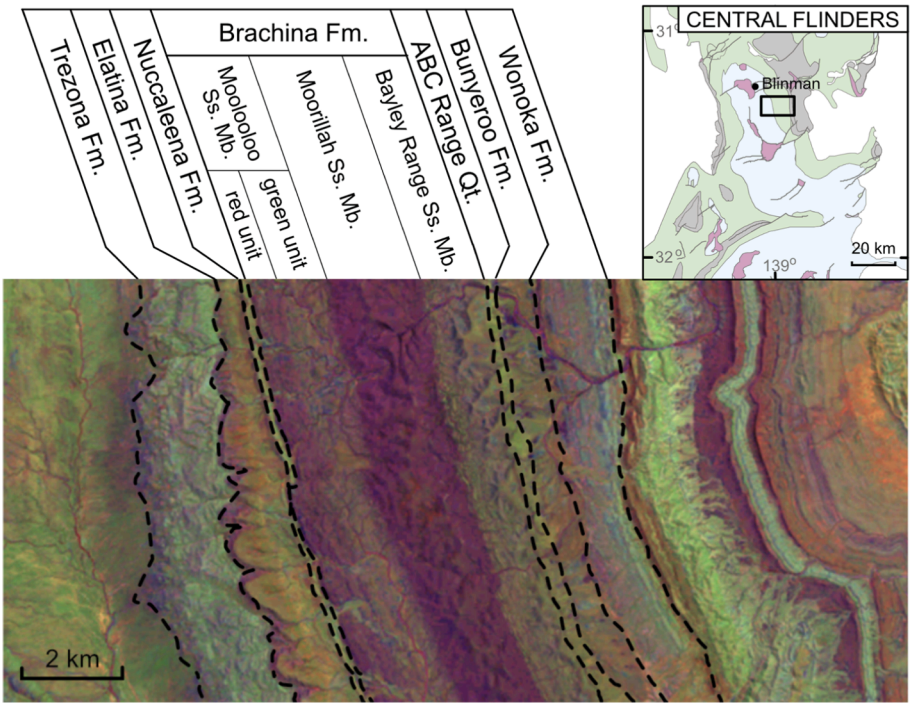

Fig. 12. Colour-filtered satellite imagery showing the Brachina Formation red unit in the Central Flinders Ranges ~ 10 km southeast of Blinman. Satellite images are from Sentinel 2, with band ratios 6/1, 11, and 3, for red, green, and blue, respectively. (For interpretation of the references to colour in this figure legend, the reader is referred to the web version of this article.)

these elements have a strong affinity for reduced sulphur and would precipitate as sulphides if any were present. A comparison between marine cement data from the Nuccaleena Formation and the Beck Spring Formation of Death Valley, USA, which is interpreted as having deposited in a euxinic environment, shows stark geochemical differences (Fig. 13). The Beck Spring Formation shows low Fe and chalcophile element (Co, Cu, Pb, Zn) concentrations, suggesting that precipitation of sulfide minerals may have scavenged these elements from solution (Shuster et al., 2018). Nuccaleena Formation marine cements have markedly higher Fe, Zn, and Cu concentrations, and appear geochemically similar to those from the Balcanoona Formation of the Cryogenian interglacial interval in the Flinders Ranges, the depositional conditions of which has been interpreted as suboxic to ferruginous.

Averaged REE profiles from all sheet cavity localities are also broadly consistent with the degree of seawater oxygenation decreasing from south to north (Fig. 9). The southernmost locality, IQ, shows an

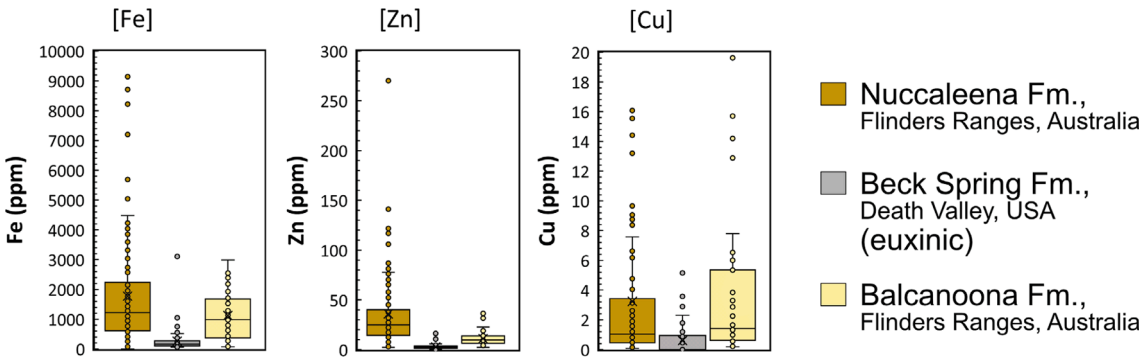

Fig. 13. Box plots comparing the concentrations of Fe, Zn, and Cu in marine cements from the Nuccaleena Formation (early Ediacaran from the Flinders Ranges; this study), the Beck Spring Formation (late Tonian from Death Valley, USA; data from Shuster et al., 2018), and the Balcanoona Formation (mid-Cryogenian from the Flinders Ranges; Hood and Wallace, 2015). The Beck Spring Formation is believed to have deposited in euxinic conditions and the Balcanoona Formation is believed to have deposited in oxic to ferruginous conditions. Boxes show interquartile range (with median marked by a horizontal line) and whiskers show range; data points outside of box and whiskers are outliers.

averaged normalised REE profile with a distinct negative Ce anomaly. Unlike most other rare earth elements, Ce is redox-sensitive. When oxidized to its tetravalent state, Ce becomes insoluble and is removed from seawater, typically through adsorption onto Mn oxyhydroxides (Moffett, 1994). This results in the Ce concentration of oxic seawater being lower relative to the neighbouring REE, La and Pr (German and Elderfield, 1990). A negative Ce anomaly in IQ marine cements is therefore consistent with oxic seawater conditions. The cements from IQ also have a depletion in light rare earth elements, and most closely (of the cements studied here) resemble Phanerozoic REE profiles from oxic marine water (Kamber, 2010).

Both IQ and CG (southern localities) averaged REE profiles also show enrichment in middle rare earth elements (MREE). Middle rare earth element enrichment can be indicative of a transition to more reducing seawater conditions, because under reduced conditions, Mn-Fe oxyhydroxides will dissolve and preferentially release MREE. This cycling occurs around the Mn-Fe redoxcline where conditions shift from oxic to anoxic (Bau et al., 1997). This explanation is consistent with Mn data from CG which also showed Mn peak concentrations and strong bright-non CL zonation, likely suggesting precipitation at the Mn^{2+}/Mn^{4+} redoxcline. The slightly positive Ce anomalies from CG are also consistent with this locality being located close to the Mn^{2+}/Mn^{4+} redoxcline. In contrast, averaged REE profiles from the two northernmost sections, LG and KC, show positive Eu anomalies and relatively flat REE profiles (i.e. they are not light REE depleted). Release of Eu^{2+} is a product of feldspar alteration at high temperatures, and as a result is commonly assumed to be associated with hydrothermal fluids (Bau, 1991). Eu is redox sensitive and in oxic conditions will quickly be converted to its trivalent form, Eu^{3+}, and adsorb to Mn-Fe oxyhydroxides (Bau, 1991). In anoxic waters, however, Eu^{2+} can stay in solution and result in positive Eu anomalies (Kamber and Webb, 2001). The presence of positive Eu anomalies and lack of any Ce anomaly in the northernmost, deeper sections is therefore consistent with the existence of an anoxic and ferruginous deep water mass in this ocean basin. Overall, these deeper water localities have REE profiles that resemble previously described Tonian and Cryogenian marine profiles (e.g., Hood and Wallace, 2015; Shuster et al., 2018).

The northwards deepening of the basin, and associated increase in the extent of anoxic marine conditions is also reflected in the carbon isotope signature of the Nuccaleena Formation. A compilation of carbon isotope profiles through this unit throughout the Central and Northern Flinders Ranges shows a general trend of $\delta^{13}C$ average composition becoming slightly more negative to the north (Fig. 14) (data from Rose and Maloof, 2010; Rose, 2012). In modern oceans, primary production of organic matter in the photic zone preferentially extracts ^{12}C from marine water and this is later released into deeper waters when the

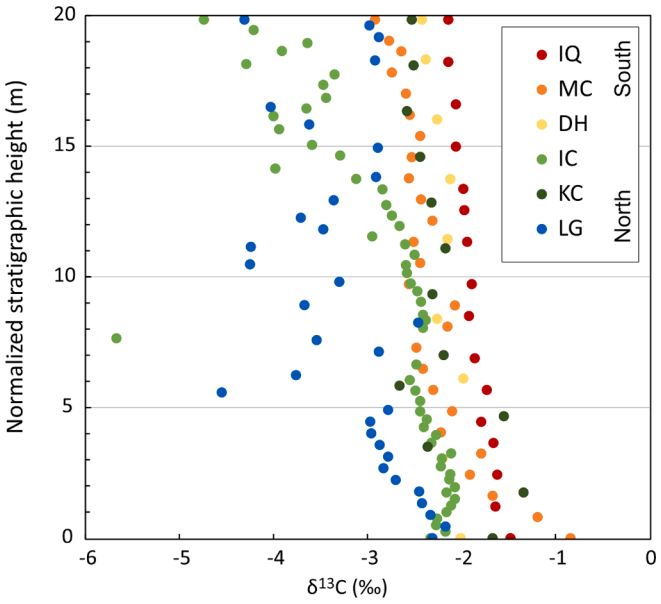

Fig. 14. Carbon isotope data from Rose (2012). Sections are labelled with nearest matching locality from this study, and were collected from the same general region within a few kilometres.

organic matter is dissolved. This produces a 1–2 ‰ depth gradient in $\delta^{13}C$ in the well-oxygenated and mixed modern ocean (Kroopnick, 1985). This "biological pump" may explain the slight gradient observed from south to north in the Nuccaleena Formation.

Sedimentological evidence from the many units in the Adelaide Superbasin indicate that the depositional environment was deepening to north during the early Ediacaran. Marine cement geochemistry from the Nuccaleena Formation shows a distribution of redox-sensitive trace elements, including Fe, Mn, U, Co, Cu, Zn, Pb, Ba, and Cd, and REE profiles indicating that the southern sections were dominated by oxic environments, while the northern sections were anoxic (Fig. 15). The colour of overlying Brachina Formation shales supports this interpretation, with red, iron-oxide-rich shales in the south and green shales in the north. Combining the sedimentological and geochemical evidence indicates that the southern and northern localities were deposited in shallower oxic and deeper anoxic-ferruginous settings, respectively.

5.3. *Temporal variation in redox geochemistry*

The spatial trends in lithology, REE patterns, trace elements, and

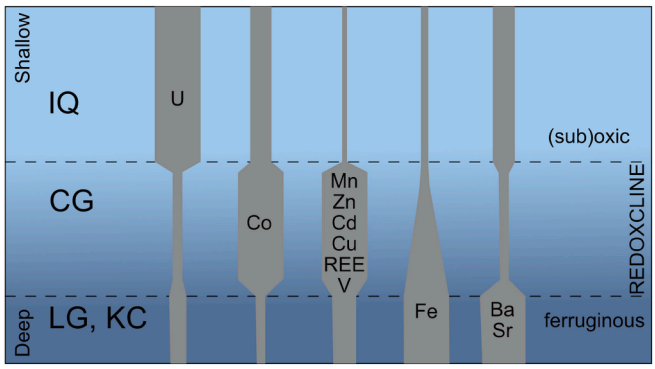

Fig. 15. Summary of trace element concentrations by relative depth, as controlled by redox conditions. See Fig. 3 for localities CG = Mount Chambers Gorge; LG = Lame Horse Gully; IQ = Ivy Queen Mine; KC = Korrowilya Creek).

$\delta^{13}C$ paint an overall picture of more oxygenated, shallow conditions to south and anoxic-ferruginous, deeper conditions to the north. However, there is also significant temporal variability in REE profiles within cement crusts in individual samples (Fig. 10).

In the shallow, southern-most localities, IQ samples show the starkest change between early marine cement REE profiles and mid to late parts of the fibrous marine cement crust. Early cement analyses show normalised REE profile shapes similar to modern seawater (e.g. compilation in Kamber, 2010), with a pronounced negative Ce anomaly and positive Y anomaly, as well overall HREE enrichment. This result suggests that the seawater these early cements precipitated from was likely oxic. REE profiles of fibrous cements further into the cavities at this locality show a strong MREE enrichment and the disappearance of the Ce and Y anomalies. This MREE enrichment is most likely to be related to Fe-oxyhydroxide dissolution, suggesting that the later fibrous cements formed under less oxic fluid conditions than the earliest fibrous cements.

The CG locality shows less drastic changes in shale-normalised REE profiles, but with a similar trend to that seen at IQ. Early marine cements show a slight negative Ce anomaly that is not present further into the fibrous cement crust, suggesting an early, short-lived period of oxygenation during precipitation. The Y anomaly becomes less prominent in later fibrous cements as well, which could also be a function of redox conditions. Ho is preferentially adsorbed onto Mn-Fe-oxyhydroxides relative to Y, resulting in a higher Y/Ho ratio under oxic conditions (Bau et al., 1997). Under anoxic conditions, when Mn-Fe-oxyhydroxides begin to dissolve, relatively higher amounts of Ho are released and the Y/Ho ratio will decrease (Bau et al., 1997; Wallace et al., 2017).

In the deeper northern parts of the basin, the LG marine cements show the Eu anomaly as more pronounced and Y/Ho as less pronounced towards the centre of the cavity, which suggests a shift to increasingly anoxic fluids during cementation. The absence of a negative Ce anomaly even in the earliest cements suggests a comparatively less oxygenated environment than the previous two localities. This interpretation is also supported by the gradual decline in HREE enrichment moving from early to later part of the marine cement crust.

There are two possible factors that could be contributing to the apparent decline in oxidation state through the marine cement crusts observed at all localities. The changes in REE profiles from margin towards the centre of the sheet cavity cements at each locality could be caused by either:

1) secular changes in seawater chemistry throughout the duration of the cement growth.
2) increasing restriction in porosity and permeability as the cement crusts grow and fill in the cavities leading to pore water anoxia.

In either case, the earliest forming cements within the sheet cavities are most likely to preserve a seawater signature representative of Nuccaleena Formation time. With progressive cementation, the cavities have less space for fluids to flow through and may become restricted, with cements then reflecting pore water rather than marine chemistry. Additionally, the cavities will become progressively buried beneath depositing sediment, which would further restrict fluid flow. However, it is likely that most of the fibrous cements formed in relatively open conditions, as large volumes of fluid flow are required for cements to grow with the observed fibrous texture (Tucker and Wright, 1990).

Though increasing restriction cannot be ruled out as a contributing factor for the changing geochemistry within the cement crusts, the earliest cements, which represent unrestricted seawater, still show a north–south redox gradient where IQ and CG cements were precipitated from oxic seawater, and KC and LG from comparatively much less oxygenated seawater.

The documented extent of the basal red unit of the Brachina Formation supports the hypothesis that changing seawater chemistry is the most likely explanation for the observed trends in the marine cements REE patterns of the Nuccaleena Formation. The systematic change in distribution and thickness of the red unit is an indication that the availability of O_2 in seawater was changing with time and depth. The red-to-green transition in the Brachina Formation therefore serves as a tracer of the Fe^{2+} / Fe^{3+} redox chemocline position during earliest Ediacaran time, and its subsequent return to shallower depths later during Mooloolooo Siltstone Member time (Fig. 16).

5.4. Implications

There has been substantial debate regarding the extent of marine oxygenation during the Ediacaran and its influence on metazoan evolution. Ediacaran oxygenation is a key part of the Neoproterozoic Oxygenation Event and there has been significant research supporting this (Canfield et al., 2007; Scott et al., 2008; Sahoo et al., 2012,2016; Partin et al., 2013). However, there is now evidence to indicate that the global oceans were not fully oxygenated until well into the Phanerozoic (Dahl et al., 2010; Sperling et al., 2015; Wallace et al., 2017). In addition, several studies have now disputed the evidence for widespread Ediacaran oxygenation (Johnston et al., 2013; Miller et al., 2017; Ostrander et al., 2020; Ostrander, 2023), and therefore the links

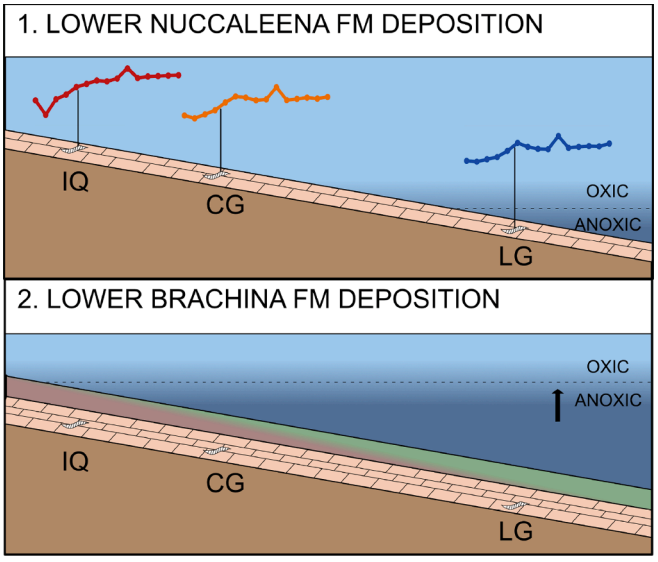

Fig. 16. Summary of early Ediacaran deposition. The lower Nuccaleena Formation is deposited while the redoxcline is deepest (1), and the redoxcline shallows over time as the Nuccaleena Formation finishes depositing and sedimentation of the Brachina Formation begins (2).

between oxygen buildup and metazoan evolution.

The oldest of the debated Ediacaran oxygenation events is the earliest Ediacaran event (Ocean Oxygenation Event A) described by Sahoo et al., (2012 and examined in this study. Multiple lines of evidence from the Adelaide Superbasin indicate the existence of a post-glacial oxic episode following the Marinoan Glaciation. Red shales are regionally developed at this stratigraphic interval over the Adelaide Superbasin (Fig. 11). The documented south to north paleodepth gradient indicates that the Fe^{2+}/Fe^{3+} chemocline was in relatively deep water (well below wave base–perhaps several hundreds of meters water depth). In addition, the trace element geochemistry (Fe, Mn, Ba, chalcophile metals, REEs) from marine dolomite cements across this paleodepth profile are consistent with a deep chemocline beneath an oxic water column. The elevated Fe and chalcophile element contents of marine cements from deeper water paleodepths (in the north) indicate the presence of a ferruginous-anoxic deep water mass.

These data provide direct evidence for an earliest Ediacaran oxic water mass penetrating to a substantial paleodepth. Evidence from South China (Sahoo et al., 2012; 2016) from a similar stratigraphic interval is consistent with this scenario and supports the notion of a redox-stratified Ediacaran ocean. Hence, while there is good evidence for a weakly oxygenated Ediacaran ocean in which deep abyssal environments were anoxic, it is likely that continental margin settings were periodically bathed in oxygenated water. This redox stratified scenario allows the possibility that increasing levels of oxygen during the Ediacaran were conducive to the evolution of metazoans, since it is likely that early metazoans (and their precursors) did evolve in such shallow marine settings. The lack of evidence for oxic marine settings in some Neoproterozoic successions globally may be due to greater paleodepths at these locations (as in North-West Canada, Johnston et al., 2013). Paleoredox proxies like shale-hosted Mo and U that have been used to monitor global oceanic redox (eg. Kunzmann et al., 2015, Miller et al., 2017) may not be very sensitive to small degrees of oxygenation where only the upper water column is oxygenated.

The ultimate cause of post-glacial oxygenation has previously been related to Marinoan deglaciation. Deglaciation and associated increased continental weathering may have caused a large influx of nutrients from terrestrial runoff to the ocean, increasing primary productivity and consequently increasing the rate of burial of organic carbon (Planavsky et al., 2010). This burial would have the effect of increasing oxygen levels following deglaciation and would provide an explanation for a post-Marinoan oxygenation event.

Significantly, the earliest marine cements of the Nuccaleena Formation record the most oxic conditions. This observation is true of all localities across the Flinders Ranges, and is most obvious in the shallower paleoenvironments of the central Flinders Ranges (localities IQ and CG). Furthermore, in the central Flinders localities, there is no transition from reduced to oxygenated conditions detectable at the base of the Nuccaleena Formation. In addition, the underlying Elatina Formation has a pink-red colour, suggesting that the marine environment was already oxic at the onset of cap deposition and that the posited oxygenation must have already begun during the Marinoan glaciation. This observation could either mean that the Marinoan glaciation was generally characterised by oxic environments, or that the later portion (perhaps the deglacial interval) of the Marinoan glaciation was oxic. In either case, the oxic episode recorded in the Nuccaleena and basal Brachina formations likely began during the Marinoan glaciation.

A potential source of oxygen to seawater during glaciation (as opposed to during deglaciation) is glacial meltwater. Glacial ice is partly made up of compacted snow containing small bubbles of air which can be released into meltwater as dissolved O_2 (Brown et al., 1994). There is evidence that even during the Snowball glaciations, meltwater from the base of the ice sheets was mixing with seawater and creating oxic zones near ice-shelf grounding lines (Lechte et al., 2019). It is therefore possible that Nuccaleena-Brachina oxic episode represents the termination of a glacially-related oxygenation episode, rather than being related strictly to deglaciation. Regardless of the direct causes for oxygenation following the Marinoan glaciation, there must have been longer term carbon-cycle processes at work during the Ediacaran and Early Paleozoic that were conducive to oceanic oxygenation.

6. Conclusions

Sedimentological and geochemical data from the basal Ediacaran Nuccaleena and Brachina Formations of the Flinders Ranges, South Australia, suggest an episode of oxygenation following the Marinoan glaciation. A red shale interval is widely developed within the basal Brachina Formation (Ediacaran Wilpena Group) of the central Flinders Ranges and this transitions into green shales northwards. The red to green shale transition corresponds with a facies change to a deeper water setting in the north, suggesting the existence of a deepwater Fe^{2+}/Fe^{3+} redox chemocline. The red-green shale transition and redox chemocline occurs in a succession dominated by shales of probable hemipelagic origin, suggesting a deep marine setting that was deposited well below storm wave base (likely several hundreds of meters depth).

The Nuccaleena Formation cap carbonate immediately underlies the red/green shale interval and contains sheet cavities with primary marine fibrous dolomite cements. Cathodoluminescence microscopy and trace element analysis of these marine dolomite cements indicates an oxic setting in the central Flinders Ranges, with cements showing non-luminescence, with low Fe-Mn concentrations and negative Ce anomalies. In the north, the marine dolomite cements have high Fe and Mn, and no Ce anomalies, indicating anoxic and ferruginous conditions. The chemistry of these marine cements is consistent with the red-green shale transition and indicates the earliest Ediacaran ocean was redox stratified with oxic water penetrating to a substantial paleodepth. However, the deeper water mass remained anoxic and ferruginous, with a chemistry similar to earlier Tonian and Cryogenian marine water.

This paleoredox data from the Adelaide Superbasin is consistent with previous studies indicating the presence of an earliest Ediacaran oxygenation event in the aftermath of the end-Cryogenian glaciation from South China. The evidence presented here suggests that, while Ediacaran abyssal settings remained anoxic and ferruginous, continental margin settings were periodically bathed in oxic waters that may have helped to promote the evolution of metazoans.

CRediT authorship contribution statement

Kelsey G. Lamothe: Writing – original draft, Investigation, Formal analysis, Data curation. **Malcolm W. Wallace:** Writing – review & editing, Writing – original draft, Supervision, Resources, Methodology, Investigation, Formal analysis, Conceptualization. **Ashleigh V.S. Hood:** Writing – review & editing, Supervision, Resources, Investigation, Funding acquisition. **Catherine V. Rose:** Writing – review & editing, Investigation.

Declaration of competing interest

The authors declare that they have no known competing financial interests or personal relationships that could have appeared to influence the work reported in this paper.

Data availability

A supplementary data spreadsheet that contains the data used in this study is provided.

Acknowledgements

A. Hood would like to acknowledge funding from an ARC DECRA (DE190100988). This research was partially funded by ARC Discovery Grant DP210103715. Field work was assisted by Jack Stacey, Elizabeth

Mahon, and John Johnson. LA-ICP-MS work was aided by Alan Greig. K. Lamothe would like to acknowledge support from an Australian Government Research Training Program Scholarship and a Baragwanath Research Scholarship.

Appendix A. Supplementary material

Supplementary data to this article can be found online at https://doi.org/10.1016/j.precamres.2024.107433.

References

Banner, J.L., Hanson, G.N., 1990. Calculation of simultaneous isotopic and trace element variations during water-rock interaction with applications to carbonate diagenesis. Geochim. Cosmochim. Acta 54 (11), 3123–3137. https://doi.org/10.1016/0016-7037(90)90128-8.

Barnaby, R.J., Rimstidt, J.D., 1989. Redox conditions of calcite cementation interpreted from Mn and Fe contents of authigenic calcites. Geol. Soc. Am. Bull. 101 (6), 795–804. https://doi.org/10.1130/0016-7606(1989)101%3C0795:RCOCCI%3E2.3.CO;2.

Bau, M., 1991. Rare-earth element mobility during hydrothermal and metamorphic fluid-rock interaction and the significance of the oxidation state of europium. Chem. Geol. 93 (3–4), 219–230. https://doi.org/10.1016/0009-2541(91)90115-8.

Bau, M., Möller, P., Dulski, P., 1997. Yttrium and lanthanides in eastern Mediterranean seawater and their fractionation during redox-cycling. Mar. Chem. 56 (1–2), 123–131. https://doi.org/10.1016/S0304-4203(96)00091-6.

Bristow, T.F., Bonifacie, M., Derkowski, A., Eiler, J.M., Grotzinger, J.P., 2011. A hydrothermal origin for isotopically anomalous cap dolostone cements from south China. Nature 474 (7349), 68–71. https://doi.org/10.1038/nature10096.

Brown, G.H., Tranter, M., Sharp, M.J., Davies, T.D., Tsiouris, S., 1994. Dissolved oxygen variations in Alpine glacial meltwaters. Earth Surf. Proc. Land. 19 (3), 247–253. https://doi.org/10.1002/esp.3290190305.

Calver, C.R., Crowley, J.L., Wingate, M.T.D., Evans, D.A.D., Raub, T.D., Schmitz, M.D., 2013. Globally synchronous Marinoan deglaciation indicated by U-Pb geochronology of the Cottons Breccia, Tasmania. Australia. *Geology* 41 (10), 1127–1130. https://doi.org/10.1130/G34568.1.

Calvert, S.E., Pedersen, T.F., 1993. Geochemistry of recent oxic and anoxic marine sediments: Implications for the geological record. Mar. Geol. 113, 67–88. https://doi.org/10.1016/0025-3227(93)90150-T.

Canfield, D.E., Poulton, S.W., Narbonne, G.M., 2007. Late-Neoproterozoic deep-ocean oxygenation and the rise of animal life. Science 315 (5808), 92–95. https://doi.org/10.1126/science.1135013.

Canfield, D.E., Teske, A., 1996. Late Proterozoic rise in atmospheric oxygen concentration inferred from phylogenetic and sulphur-isotope studies. Nature 382, 127–132. https://doi.org/10.1038/382127a0.

Coats, R.P., Blissett, A.H., 1971. Regional and economic geology of the Mount Painter Province (Vol. 43). Department of Mines, Geological Survey of South Australia.

Cole, D.B., Reinhard, C.T., Wang, X., Gueguen, B., Halverson, G.P., Gibson, T., Hodgskiss, M.S., McKenzie, N.R., Lyons, T.W., Planavsky, N.J., 2016. A shale-hosted Cr isotope record of low atmospheric oxygen during the Proterozoic. Geology 44, 555–558. https://doi.org/10.1130/G37787.1.

Compston, W., Williams, I.S., Jenkins, R.J.F., Gostin, V.A., Haines, P.W., 1987. Zircon age evidence for the Late Precambrian Acraman ejecta blanket. Aust. J. Earth Sci. 34 (4), 435–445. https://doi.org/10.1080/08120098708729424.

Corkeron, M., 2007. 'Cap carbonates' and Neoproterozoic glacigenic successions from the Kimberley region, north-west Australia. Sedimentology 54, 871–903. https://doi.org/10.1111/j.1365-3091.2007.00864.x.

Dahl, T.W., Hammarlund, E.U., Anbar, A.D., Bond, D.P., Gill, B.C., Gordon, G.W., Knoll, A.H., Nielsen, A.T., Schovsbo, N.H., Canfield, D.E., 2010. Devonian rise in atmospheric oxygen correlated to the radiations of terrestrial plants and large predatory fish. Proc. Natl. Acad. Sci. 107, 17911–17915. https://doi.org/10.1073/pnas.1011287107.

Dalgarno, C.R., Johnson, J.E., 1964. The Wilpena Group. Precambrian rock groups in the Adelaide Geosyncline: a new subdivision. Quarterly Geological Notes, Geological Survey of South Australia 20, 12–15.

de Baar, H.J., German, C.R., Elderfield, H., Van Gaans, P., 1988. Rare earth element distributions in anoxic waters of the Cariaco Trench. Geochim. Cosmochim. Acta 52 (5), 1203–1219. https://doi.org/10.1016/0016-7037(88)90275-X.

Dyson, I.A., 1992. Stratigraphic nomenclature and sequence stratigraphy of the lower Wilpena Group, Adelaide Geosyncline: the Sandison Subgroup. Quarterly Geological Notes, Geological Survey of South Australia 122, 2–13.

Dyson, I.A., 2002. The Port Stanvac sandstone member of the Upper Brachina Formation and its relationship to the ABC Range Quartzite. MESA J. 26, 42–50.

Fairchild, I.J., Bao, H., Windmill, R., Boomer, I., 2023. The Marinoan cap carbonate of Svalbard: syngenetic marine dolomite with relic 17O carbonate-associated sulphate anomaly. The Depositional Record. 9, 482–507. https://doi.org/10.1002/dep2.201.

Fike, D.A., Grotzinger, J.P., Pratt, L.M., Summons, R.E., 2006. Oxidation of the Ediacaran ocean. Nature 444 (7120), 744–747. https://doi.org/10.1038/nature05345.

Font, E., Nédélec, A., Trindade, R.I.F.D., Moreau, C., 2010. Fast or slow melting of the Marinoan snowball Earth? The cap dolostone record. Palaeogeogr. Palaeoclimatol. Palaeoecol. 295 (1–2), 215–225. https://doi.org/10.1016/j.palaeo.2010.05.039.

Fromhold, T., Wallace, M., 2012. Regional recognition of the Neoproterozoic Sturtian,-Marinoan boundary, Northern and Central Adelaide Geosyncline, South Australia. Aust. J. Earth Sci. 59, 527–546. https://doi.org/10.1080/08120099.2012.673507.

Gan, T., Zhou, G., Luo, T., Pang, K., Zhou, M., Luo, W., Wang, S., Xiao, S., 2022. Earliest Ediacaran speleothems and their implications for terrestrial life after the Marinoan snowball Earth. Precambr. Res. 376, 106685 https://doi.org/10.1016/j.precamres.2022.106685.

German, C.R., Elderfield, H., 1990. Application of the Ce anomaly as a paleoredox indicator: the ground rules. Paleoceanography 5 (5), 823–833. https://doi.org/10.1029/PA005i005p00823.

Hardisty, D.S., Lu, Z., Bekker, A., Diamond, C.W., Gill, B.C., Jiang, G., Kah, L.C., Knoll, A. H., Loyd, S.J., Osburn, M.R., 2017. Perspectives on Proterozoic surface ocean redox from iodine contents in ancient and recent carbonate. Earth Planet. Sci. Lett. 463, 159–170. https://doi.org/10.1016/j.epsl.2017.01.032.

Harms, J.C., Southard, J.B., Spearing, D.R., Walker, R.G., 1975. Depositional environments as interpreted from primary sedimentary structures and stratification sequences. SEPM Soc. Sediment. Geol. Short Course 2, 161p. https://doi.org/10.2110/scn.75.02.

Hoffman, P.F., 2011. Strange bedfellows: glacial diamictite and cap carbonate from the Marinoan (635 Ma) glaciation in Namibia. Sedimentology 58 (1), 57–119. https://doi.org/10.1111/j.1365-3091.2010.01206.x.

Hoffman, P.F., Li, Z.X., 2009. A palaeogeographic context for Neoproterozoic glaciation. Palaeogeogr. Palaeoclimatol. Palaeoecol. 277 (3–4), 158–172. https://doi.org/10.1016/j.palaeo.2009.03.013.

Hoffman, P.F., Macdonald, F.A., 2010. Sheet-crack cements and early regression in Marinoan (635 Ma) cap dolostones: regional benchmarks of vanishing ice-sheets? Earth Planet. Sci. Lett. 300 (3–4), 374–384. https://doi.org/10.1016/j.epsl.2010.10.027.

Hoffman, P.F., Schrag, D.P., 2002. The snowball Earth hypothesis: testing the limits of global change. Terra Nova 14 (3), 129–155. https://doi.org/10.1046/j.1365-3121.2002.00408.x.

Holland, H.D., 2002. Volcanic gases, black smokers, and the Great Oxidation Event. Geochim. Cosmochim. Acta 66, 3811–3826. https://doi.org/10.1016/S0016-7037(02)00950-X.

Holland, H.D., 2006. The oxygenation of the atmosphere and oceans. Philos. Trans. R. Soc., B 361 (1470), 903–915. https://doi.org/10.1098/rstb.2006.1838.

Hood, A.v.S., Wallace, M.W., 2012. Synsedimentary diagenesis in a Cryogenian reef complex: Ubiquitous marine dolomite precipitation. *Sedimentary Geology, 255*, pp.56-71. Doi: 10.1016/j.sedgeo.2012.02.004.

Hood, A.V.S., Wallace, M.W., 2015. Extreme ocean anoxia during the Late Cryogenian recorded in reefal carbonates of Southern Australia. Precambr. Res. 261, 96–111. https://doi.org/10.1016/j.precamres.2015.02.008.

Hood, A.V.S., Wallace, M.W., 2018. Neoproterozoic marine carbonates and their paleoceanographic significance. Global Planet. Change 160, 28–45. https://doi.org/10.1016/j.gloplacha.2017.11.006.

Hu, Y., Cai, C., Sun, P., Zhang, H., Liu, Z., Li, Y., Wang, Q., Tang, Y., Immenhauser, A., 2023. Palaeo-environmental significance of fibrous carbonate cement in Marinoan cap carbonates. Mar. Pet. Geol. 155, 106392 https://doi.org/10.1016/j.marpetgeo.2023.106392.

Jiang, G., Kennedy, M.J., Christie-Blick, N., 2003. Stable isotopic evidence for methane seeps in Neoproterozoic postglacial cap carbonates. Nature 426 (6968), 822–826. https://doi.org/10.1038/nature02201.

Jiang, G., Kennedy, M.J., Christie-Blick, N., Wu, H., Zhang, S., 2006. Stratigraphy, sedimentary structures, and textures of the late Neoproterozoic Doushantuo cap carbonate in South China. J. Sediment. Res. 76 (7), 978–995. https://doi.org/10.2110/jsr.2006.086.

Johnston, D.T., Poulton, S.W., Tosca, N.J., O'brien, T., Halverson, G.P., Schrag, D.P., Macdonald, F.A., 2013. Searching for an oxygenation event in the fossiliferous Ediacaran of northwestern Canada. *Chemical Geology, 362*, pp.273-286. Doi: 10.1016/j.chemgeo.2013.08.046.

Kamber, B.S., 2010. Archean mafic–ultramafic volcanic landmasses and their effect on ocean–atmosphere chemistry. Chem. Geol. 274 (1–2), 19–28. https://doi.org/10.1016/j.chemgeo.2010.03.009.

Kamber, B.S., Webb, G.E., 2001. The geochemistry of late Archaean microbial carbonate: implications for ocean chemistry and continental erosion history. Geochim. Cosmochim. Acta 65 (15), 2509–2525. https://doi.org/10.1016/S0016-7037(01)00613-5.

Kennedy, M.J., 1996. Stratigraphy, sedimentology, and isotopic geochemistry of Australian Neoproterozoic postglacial cap dolostones; deglaciation, delta 13 C excursions, and carbonate precipitation. J. Sediment. Res. 66 (6), 1050–1064. https://doi.org/10.2110/jsr.66.1050.

Kennedy, M.J., Christie-Blick, N., Sohl, L.E., 2001. Are Proterozoic cap carbonates and isotopic excursions a record of gas hydrate destabilization following Earth's coldest intervals? Geology 29 (5), 443–446. https://doi.org/10.1130/0091-7613(2001)029%3C0443:APCCAI%3E2.0.CO;2.

Kilner, B., Niocaill, C., Brasier, M., 2005. Low-latitude glaciation in the Neoproterozoic of Oman. Geology 33 (5), 413–416. https://doi.org/10.1130/G21227.1.

Knoll, A.H., Javaux, E.J., Hewitt, D., Cohen, P., 2006. Eukaryotic organisms in Proterozoic oceans. Philos. Trans. R. Soc., B 361 (1470), 1023–1038. https://doi.org/10.1098/rstb.2006.1843.

Kroopnick, P.M., 1985. The distribution of ^{13}C of ΣCO_2 in the world oceans. Deep Sea Research Part A Oceanographic Research Papers 32, 57–84. https://doi.org/10.1016/0198-0149(85)90017-2.

Kunzmann, M., Halverson, G.P., Scott, C., Minarik, W.G., Wing, B.A., 2015. Geochemistry of Neoproterozoic black shales from Svalbard: Implications for

oceanic redox conditions spanning Cryogenian glaciations. Chem. Geol. 417, 383–393. https://doi.org/10.1016/j.chemgeo.2015.10.022.
Langmuir, D., 1978. Uranium solution-mineral equilibria at low temperatures with applications to sedimentary ore deposits. Geochim. Cosmochim. Acta 42 (6), 547–569. https://doi.org/10.1016/0016-7037(78)90001-7.
Lawrence, M.G., Greig, A., Collerson, K.D., Kamber, B.S., 2006. Rare earth element and yttrium variability in South East Queensland waterways. Aquat. Geochem. 12, 39–72. https://doi.org/10.1007/s10498-005-4471-8.
Lechte, M.A., Wallace, M.W., Hood, A.V.S., Li, W., Jiang, G., Halverson, G.P., Asael, D., McColl, S.L., Planavsky, N.J., 2019. Subglacial meltwater supported aerobic marine habitats during Snowball Earth. Proc. Natl. Acad. Sci. 116 (51), 25478–25483. https://doi.org/10.1073/pnas.1909165116.
Leeson, B., 1970. Geology of the Beltana 1:63,360 map area. Report of Investigations, No, p. 35.
Lemon, N. M., 1988. Diapir recognition and modelling with examples from the late Proterozoic Adelaide Geosyncline, central Flinders Ranges, South Australia. (PhD Thesis, University of Adelaide, Dept. of Geology and Geophysics).
Lyons, T.W., Reinhard, C.T., Planavsky, N.J., 2014. The rise of oxygen in Earth's early ocean and atmosphere. Nature 506 (7488), 307–315. https://doi.org/10.1038/nature13068.
McKirdy, D.M., Burgess, J.M., Lemon, N.M., Yu, X., Cooper, A.M., Gostin, V.A., Jenkins, R.J., Both, R.A., 2001. A chemostratigraphic overview of the late Cryogenian interglacial sequence in the Adelaide Fold-Thrust Belt. South Australia. *Precambrian Research* 106 (1–2), 149–186. https://doi.org/10.1016/S0301-9268(00)00130-3.
Mclennan, S.M., 1989. Rare earth elements in sedimentary rocks; influence of provenance and sedimentary processes. Rev. Mineral. Geochem. 21 (1), 169–200.
Miller, A.J., Strauss, J.V., Halverson, G.P., Macdonald, F.A., Johnston, D.T., Sperling, E. A., 2017. Tracking the onset of Phanerozoic-style redox-sensitive trace metal enrichments: new results from basal Ediacaran post-glacial strata in NW Canada. Chem. Geol. 457, 24–37. https://doi.org/10.1016/j.chemgeo.2017.03.010.
Mirams, R.C., 1964. BURRA map sheet, Geological Atlas of South Australia, 1: 250 000 series. Geol. Surv. S, Aust.
Moffett, J.W., 1994. A radiotracer study of cerium and manganese uptake onto suspended particles in Chesapeake Bay. Geochim. Cosmochim. Acta 58 (2), 695–703. https://doi.org/10.1016/0016-7037(94)90499-5.
Narbonne, G.M., Gehling, J.G., 2003. Life after snowball: the oldest complex Ediacaran fossils. Geology 31 (1), 27–30. https://doi.org/10.1130/0091-7613(2003)031%3C0027:LASTOC%3E2.0.CO;2.
O'Connell, B., Wallace, M.W., Hood, A.V., Lechte, M.A., Planavsky, N.J., 2020. Iron-rich carbonate tidal deposits, Angepena Formation, South Australia: a redox-stratified Cryogenian basin. Precambr. Res. 342, 105668 https://doi.org/10.1016/j.precamres.2020.105668.
Ostrander, C.M., 2023. Mulling and nulling the coeval rise of Ediacaran oxygen and animals. Earth Planet. Sci. Lett. 614, 118187 https://doi.org/10.1016/j.epsl.2023.118187.
Ostrander, C.M., Owens, J.D., Nielsen, S.G., Lyons, T.W., Shu, Y., Chen, X., Sperling, E.A., Jiang, G., Johnston, D.T., Sahoo, S.K., 2020. Thallium isotope ratios in shales from South China and northwestern Canada suggest widespread O2 accumulation in marine bottom waters was an uncommon occurrence during the Ediacaran Period. Chem. Geol. 557, 119856 https://doi.org/10.1016/j.chemgeo.2020.119856.
Partin, C.A., Bekker, A., Planavsky, N.J., Scott, C., Gill, B.C., Li, C., Podkovyrov, V., Maslov, A., Konhauser, K.O., Lalonde, S.V., 2013. Large-scale fluctuations in Precambrian atmospheric and oceanic oxygen levels from the record of U in shales. Earth Planet. Sci. Lett. 369, 284–293. https://doi.org/10.1016/j.epsl.2013.03.031.
Paton, C., Hellstrom, J., Paul, B., Woodhead, J., Hergt, J., 2011. Iolite: Freeware for the visualisation and processing of mass spectrometric data. J. Anal. At. Spectrom 26 (12), 2508–2518.
Planavsky, N.J., Rouxel, O.J., Bekker, A., Lalonde, S.V., Konhauser, K.O., Reinhard, C.T., Lyons, T.W., 2010. The evolution of the marine phosphate reservoir. Nature 467 (7319), 1088–1090. https://doi.org/10.1038/nature09485.
Plummer, P.S., 1978a. Stratigraphy of the Lower Wilpena Group (Late Precambrian), Flinders Ranges, South Australia. Trans. R. Soc. S. Aust. 102, 25–38.
Plummer, P.S., 1978b. Note on the palaeoenvironmental significance of the Nuccaleena Formation (upper Precambrian), central Flinders Ranges, South Australia. J. Geol. Soc. Aust. 25, 395–402. https://doi.org/10.1080/00167617808729049.
Preiss, W.V., 1973. Palaeoecological interpretations of South Australian Precambrian stromatolites. J. Geol. Soc. Aust. 19, 501–532. https://doi.org/10.1080/00167617308728820.
Preiss, W.V., 1987. The Adelaide Geosyncline-Late Proterozoic Stratigraphy, Sedimentation. Palaeontology and Tectonics. Bull. Geol. Surv. S, Aust, p. 53.
Preiss, W.V., 2000. The Adelaide Geosyncline of South Australia and its significance in Neoproterozoic continental reconstruction. Precambr. Res. 100 (1–3), 21–63. https://doi.org/10.1016/S0301-9268(99)00068-6.
Preiss, W.V., Dyson, I.A., Reid, P.W., Cowley, W.M., 1998. Revision of lithostratigraphic classification of the Umberatana Group. Mesa Journal 9, 36–42.
Raub, T.D., Evans, D.A.D., Smirnov, A.V., 2007. Siliciclastic prelude to Elatina-Nuccaleena deglaciation: lithostratigraphy and rock magnetism of the base of the Ediacaran system. Geol. Soc. Lond. Spec. Publ. 286 (1), 53–76. https://doi.org/10.1144/SP286.5.
Reinhard, C.T., Planavsky, N.J., Olson, S.L., Lyons, T.W., Erwin, D.H., 2016. Earth's oxygen cycle and the evolution of animal life. Proc. Natl. Acad. Sci. 113 (32), 8933–8938. https://doi.org/10.1073/pnas.1521544113.
Rose, C.V., Maloof, A.C., 2010. Testing models for post-glacial 'cap dolostone'deposition: Nuccaleena Formation, South Australia. Earth Planet. Sci. Lett. 296 (3–4), 165–180. https://doi.org/10.1016/j.epsl.2010.03.031.
Rose, C.V., 2012. *Comings and goings of the end-Cryogenian ice sheet: A stratigraphic study of the pre-, syn-, and post-glacial deposits, South Australia* (Doctoral dissertation, Princeton University).
Sahoo, S.K., Planavsky, N.J., Kendall, B., Wang, X., Shi, X., Scott, C., Anbar, A.D., Lyons, T.W., Jiang, G., 2012. Ocean oxygenation in the wake of the Marinoan glaciation. Nature 489 (7417), 546–549. https://doi.org/10.1038/nature11445.
Sahoo, S.K., Planavsky, N.J., Jiang, G., Kendall, B., Owens, J.D., Wang, X., Shi, X., Anbar, A.D., Lyons, T.W., 2016. Oceanic oxygenation events in the anoxic Ediacaran ocean. Geobiology 14 (5), 457–468. https://doi.org/10.1111/gbi.12182.
Scott, C., Lyons, T.W., Bekker, A., Shen, Y., Poulton, S.W., Chu, X.-L., Anbar, A.D., 2008. Tracing the stepwise oxygenation of the Proterozoic ocean. Nature 452. https://doi.org/10.1038/nature06811 pp,456–459.
Shi, W., Mills, B.J., Li, C., Poulton, S.W., Krause, A.J., He, T., Zhou, Y., Cheng, M., Shields, G.A., 2022. Decoupled oxygenation of the Ediacaran ocean and atmosphere during the rise of early animals. Earth Planet. Sci. Lett. 591, 117619 https://doi.org/10.1016/j.epsl.2022.117619.
Shields, G.A., 2005. Neoproterozoic cap carbonates: a critical appraisal of existing models and the plumeworld hypothesis. Terra Nova 17 (4), 299–310. https://doi.org/10.1111/j.1365-3121.2005.00638.x.
Shuster, A.M., Wallace, M.W., Hood, A.v.S., Jiang, G., 2018. The Tonian Beck Spring Dolomite: Marine dolomitization in a shallow, anoxic sea. *Sedimentary Geology, 368*, pp.83-104. Doi: 10.1016/j.sedgeo.2018.03.003.
Song, H., Jiang, G., Poulton, S.W., Wignall, P.B., Tong, J., Song, H., An, Z., Chu, D., Tian, L., She, Z., Wang, C., 2017. The onset of widespread marine red beds and the evolution of ferruginous oceans. Nat. Commun. 8 (1), 399. https://doi.org/10.1038/s41467-017-00502-x.
Sperling, E.A., Wolock, C.J., Morgan, A.S., Gill, B.C., Kunzmann, M., Halverson, G.P., Macdonald, F.A., Knoll, A.H., Johnston, D.T., 2015. Statistical analysis of iron geochemical data suggests limited late Proterozoic oxygenation. Nature 523, 451–454. https://doi.org/10.1038/nature14589.
Tostevin, R., Mills, B.J., 2020. Reconciling proxy records and models of Earth's oxygenation during the Neoproterozoic and Palaeozoic. Interface Focus 10 (4), 20190137. https://doi.org/10.1098/rsfs.2019.0137.
Trindade, R.I.F.D., Font, E., D'Agrella-Filho, M.S., Nogueira, A.C.R., Riccomini, C., 2003. Low-latitude and multiple geomagnetic reversals in the Neoproterozoic Puga cap carbonate. Amazon Craton. *Terra Nova* 15 (6), 441–446. https://doi.org/10.1046/j.1365-3121.2003.00510.x.
Tucker and Wright, 1990. Carbonate Sedimentology. Blackwell Scientific Publications, pp. 1–27.
Wallace, M.W., Shuster, A., Greig, A., Planavsky, N.J., Reed, C.P., 2017. Oxygenation history of the Neoproterozoic to early Phanerozoic and the rise of land plants. Earth Planet. Sci. Lett. 466, 12–19. https://doi.org/10.1016/j.epsl.2017.02.046.
Wallace, M.W., Hood, A., Fayle, J., Hordern, E.S., O'Hare, T.F., 2019. Neoproterozoic marine dolomite hardgrounds and their relationship to cap dolomites. Precambr. Res. 328, 269–286. https://doi.org/10.1016/j.precamres.2019.04.026.
Wang, J., Jiang, G., Xiao, S., Li, Q., Wei, Q., 2008. Carbon isotope evidence for widespread methane seeps in the ca. 635 Ma Doushantuo cap carbonate in south China. Geology 36 (5), 347–350. https://doi.org/10.1130/G24513A.1.
Webb, A.W., 1981. Geochronology of the Stuart Shelf- Amdel progress report 3. S. Aust. Dept Mines and Energy Open File Env, 3859 (unpublished.
Woodhead, J.D., Hellstrom, J., Hergt, J.M., Greig, A., Maas, R., 2007. Isotopic and elemental imaging of geological materials by laser ablation inductively coupled plasma-mass spectrometry. Geostand. Geoanal. Res. 31 (4), 331–343. https://doi.org/10.1111/j.1751-908X.2007.00104.x.
Zhang, F., Xiao, S., Romaniello, S.J., Hardisty, D., Li, C., Melezhik, V., Pokrovsky, B., Cheng, M., Shi, W., Lenton, T.M., 2019. Global marine redox changes drove the rise and fall of the Ediacara biota. Geobiology 17, 594–610. https://doi.org/10.1111/gbi.12359.
Zhou, C., Bao, H., Peng, Y., Yuan, X., 2010. Timing the deposition of 17O-depleted barite at the aftermath of Nantuo glacial meltdown in South China. Geology 38 (10), 903–906. https://doi.org/10.1130/G31224.1.